International Journal of Heat and Mass Transfer 224 (2024) 125376

Contents lists available at ScienceDirect

International Journal of Heat and Mass Transfer

journal homepage: www.elsevier.com/locate/ijhmt

Flow boiling pressure drop correlation in small to micro passages

Ali H. Al-Zaidi [a], Mohamed M. Mahmoud [b], Tassos G. Karayiannis [c,*]

[a] University of Misan, Al-Amarah 62001, Iraq
[b] Faculty of Engineering, Zagazig University, Zagazig 44519, Egypt
[c] Department of Mechanical and Aerospace Engineering, Brunel University London, Uxbridge UB8 3PH, United Kingdom

ARTICLE INFO

Keywords:
Microchannels
Tubes
Pressure drop
Two-phase flow
Correlations
Acceleration component
Frictional component
Gravitational component
Lockhart–Martinelli parameter
Void fraction

ABSTRACT

An accurate and acceptable correlation for the prediction of two-phase pressure drop is considered a crucial step in heat exchanger design. Although many existing models and correlations were developed and proposed in the past, their ability to predict within acceptable error bands when applied in general to flow boiling flows is limited, even within their originally recorded ranges. The discrepancies are worse when predicting two-phase pressure drop in small to micro-scale passages. Therefore, the aim of the work described in this paper is to assess the most well-known models and correlations using a large experimental data-bank. The data-bank includes four refrigerants, namely R134a, R245fa, HFE-7100 and HFE-7200, small to micro heat exchangers made of different metals and different channel configurations. In addition, the data cover a large range of operating conditions, which can allow generally applicability of new correlations developed. This range covers channel hydraulic diameter of 0.46−4.26 mm, heated length of 20−500 mm, system pressure of 1 − 14 bar, mass flux of 50−700 kg/m^2 s, wall heat flux ranging from 2 to 234 kW/m^2 and exit vapour quality up to one. Twenty six existing models and correlations that were developed and proposed for vertical/horizontal flow, single/multi-channels and circular/non-circular channels were evaluated. Moreover, the effect of using different equations for calculating the two-phase mixture viscosity, void fraction, Fanning friction factor and Lockhart–Martinelli parameter was assessed and discussed. The mean absolute error of the existing correlations when compared with our data-bank was more than 30 %. Therefore, a new correlation for calculating the two-phase multiplier, which was strongly dependent on the Boiling number and the Lockhart–Martinelli parameter, was developed and then the frictional component and total two-phase pressure drop relationships were completed.

1. Introduction

Two-phase flow boiling is very effective in cooling high heat flux equipment because it can provide high heat transfer rates at lower mass flow rate, compared to single-phase liquid cooling. Additionally, it can keep the surface temperature uniform (slightly above the saturation temperature of the cooling liquid), which may reduce the material thermal stresses, especially in electronics cooling applications. This means that high heat fluxes can be dissipated with a lower pumping power. In addition to electronics cooling, two-phase flow boiling is encountered in several applications such as power plants, refrigeration systems and nuclear reactors. The proper design of heat exchangers used in micro-scale boiling applications requires a full understanding of two-phase flow pressure drop and heat-transfer phenomena to develop accurate prediction correlations (design equations). Therefore, significant effort has been made by the academic community to develop and propose correlations for the prediction of heat transfer rates and pressure drop at micro-scale. The accuracy of any proposed correlation can significantly affect the expected actual thermal performance of the designed heat exchanger during operation and the cost of the thermal system, e.g., inaccurate model/correlation may increase the system cost through oversizing the heat transfer equipment. It is well-known that pressure drop calculations are required for the design of any cooling system to help calculate the power consumption by the pump/compressor. This can successfully be done when a suitable correlation is selected for calculating the two-phase pressure drop.

In literature, there are several models/correlations that were developed for predicting two-phase pressure drop. Some of these correlations were proposed for conventional scale (large diameter flow passages), while others were suggested for micro-scale (small to micro diameter flow passages). However, comparing these models/correlations against each other indicates that there are large discrepancies, see Section 2. This discrepancy may be due to several factors such as different

* Corresponding author at: Department of Mechanical and Aerospace Engineering, Brunel University London, Uxbridge, Middlesex UB8 3PH, United Kingdom.
E-mail address: tassos.karayiannis@brunel.ac.uk (T.G. Karayiannis).

https://doi.org/10.1016/j.ijheatmasstransfer.2024.125376
Received 23 October 2023; Received in revised form 24 January 2024; Accepted 23 February 2024
Available online 1 March 2024

Nomenclature

a	Experimental exponent, [-]
A	Area, [m^2]
A	Single-phase frictional pressure gradient for liquid, $A = (2f_{lo}G^2)/(D_h\rho_l)$
b	Experimental exponent, [-]
B	Single-phase frictional pressure gradient for vapour, $B = (2f_{go}G^2)/(D_h\rho_g)$
Bd	Bond number, [-], $Bd = \Delta\rho g D^2/\sigma$
Bo	Boiling number, [-], $Bo = q''_w/Gi_{lg}$
c	Experimental exponent, [-]
C	Chisholm parameter, [-]
Co	Confinement number, [-], $Co = [\sigma/g\Delta\rho]^{0.5}/D$
d	Experimental exponent, [-]
D	Diameter, [m]
D_h	Hydraulic diameter, [m], $D_h = 2H_{ch}W_{ch}/(H_{ch} + W_{ch})$
DR	Density ratio, [-], $DR = \rho_l/\rho_g$
E	Dimensionless number, [-]
f	Fanning friction factor, [-]
F	Dimensionless number, [-]
Fr	Froude number, [-], $Fr = v_l^2G^2/gD$
G	Mass flux, [kg/m^2 s], $G = \dot{m}/A_{sec}N$
g	Gravitational acceleration, [m/s^2]
H	Height, [m]
H	Pressure drop ratio, [-], $H = (f_{lo}/f_{go})(\rho_g/\rho_l)$
I	Current, [Amp.]
i_{lg}	Latent heat of vaporization, [J/kg]
J_g	Superficial vapour velocity, [m/s], $J_g = Gx/\rho_g$
J_l	Superficial liquid velocity, [m/s], $J_l = G(1-x)/\rho_l$
L	Length, [m]
La	Laplace number, [-], $La = [\sigma/g(\rho_l - \rho_g)]^{0.5}$
MAE	Mean absolute error, [%]
$\dot{m}$	Mass flow rate, [kg/s]
N	Number of channels, number of data points, [-]
$N\mu$	Viscosity number, [-]
P	Pressure, [Pa]
Per	Perimeter, [m]
Q_{loss}	Heat loss, [W]
q''	Heat flux, [W/m^2]
R	Reynolds number ratio, [-], $R = Re_{lo}/Re_{go}$
Re_{lo}	Liquid only Reynolds number, [-], $Re_{lo} = GD/\mu_l$
Re_{go}	Vapour only Reynolds number, [-], $Re_{go} = GD/\mu_g$
Re_{ls}	Superficial Liquid Reynolds number, [-], $Re_{ls} = G(1-x)D/\mu_l$
Re_{gs}	Superficial vapour Reynolds number, [-], $Re_{gs} = GxD/\mu_g$
Re_{tp}	Two-phase Reynolds number, [-], $Re_{tp} = GD/\mu_{tp}$
Re^*	Laminar equivalent Reynolds number, [-]
RP	Reduced pressure, [-], $RP = P_i/P_{cr}$
Su_{lo}	Liquid only Suratman number, [-], $Su_{lo} = \rho_l\sigma D/\mu_l^2$
Su_{go}	Vapour only Suratman number, [-], $Su_{go} = \rho_g\sigma D/\mu_g^2$
T	Temperature, [K]
v	Specific volume, [m^3/kg]
V	Voltage, [volt]
W	Width, [m]
We_{lo}	Liquid only Weber number, [-], $We_{lo} = G^2D/\rho_l\sigma$
We_{go}	Vapour only Weber number, [-], $We_{go} = G^2D/\rho_g\sigma$
We_{ls}	Weber number based on the liquid superficial velocity, [-], $We_{ls} = D\rho_l J_l^2/\sigma$
We_{gs}	Weber number based on the vapour superficial velocity, [-], $We_{gs} = D\rho_g J_g^2/\sigma$
We_{tp}	Two-phase Weber number, [-],$We_{tp} = G^2D/\rho_{tp}\sigma$
X	Martinelli parameter, [-], $X = [(dP/dz)_l/(dP/dz)_g]^{0.5}$
x	Vapour quality, [-]

Greek Symbols

α	Void fraction, [-]
β	Aspect ratio, [-], β = short (width or height)/long (width or height)
ΔP	Pressure drop, [Pa]
θ	Contact angle, channel orientation, [degree]
θ	Percentage of predictions within ±30 % of data, [%]
μ	Viscosity, [Pa s]
ρ	Density, [kg/m^3]
σ	Surface tension, [N/m]
$\Ø$	Two-phase multiplier, [-]
ζ	Surface area density, [m^2/m^3]

Subscript

b	Base
acc	Acceleration
ch	Channel
cr	Critical
exp	Experimental
fr	Friction
g	Vapour or gravitational
h	Heated
i	Inner, inlet
k	Refers to l for saturated liquid or g for saturated vapour
l	Liquid
lg	Liquid-vapour
ll	Laminar liquid-laminar vapour
lo	Liquid only
lt	Laminar liquid-turbulent vapour
$meas$	Measured
o	Outlet
$pred$	Predicted
s	Superficial
sec	Cross-section
sp	Single-phase
sys	System
tl	Turbulent liquid-laminar vapour
tp	Two-phase
tt	Turbulent liquid-turbulent vapour
w	Wall, wetted

operating conditions, working fluids, channel geometry, channel size, surface material, channel configuration (single or multi-channels), channel orientation, flow stability/instability and experimental methodology (including careful system validation and degassing process). The next paragraph summarizes the effect of different parameters on the measured two-phase flow pressure drop.

Some researchers [1–7] studied the effect of mass and heat flux and reported that the two-phase pressure drop increases with increasing mass flux and heat flux (or exit vapour quality). Increasing the heat flux leads to rapid bubble generation, which increases the flow resistance and in turn the pressure drop. The increase of pressure drop with increasing mass fluxes may be attributed to the large shear stresses at the

wall and the liquid-vapour interface. Some other researchers [8–11] investigated the effect of system pressure (inlet or saturation pressure in the channels) and found that the two-phase pressure drop decreases as the system pressure increases. This may be due to the effect of pressure on fluid properties, i.e. as the pressure increases, the surface tension and liquid viscosity decreases while the vapour density increases, resulting in a reduction in the acceleration and frictional pressure drop components. Another group of researchers [12–14] studied the effect of inlet sub-cooling and agreed that the two-phase pressure drop decreases with increasing inlet sub-cooling (decreasing fluid inlet temperature). This was attributed by Lee and Karayiannis [14] to the delay in flow pattern transitions and the small void fraction as the inlet sub-cooling increases. The effect of channel diameter on pressure drop was discussed by Revellin and Thome [15], Pamitran et al. [16] and Mahmoud et al. [2] reporting that the reduction in channel diameter leads to higher two-phase pressure drop. Mahmoud et al. [2] reported as an explanation that large wall shear stress due to large velocity gradient in these passages could increase the frictional pressure drop component. The effect of channel aspect ratio or channel width on pressure drop was studied by Harirchian and Garimella [5] and researchers [17–20] and found that the smaller aspect ratio (smaller channel width) the larger the two-phase pressure drop. This was attributed by Al-Zaidi at al. [20] to the different heat transfer area in multi-channel heat sinks (due to different aspect ratio), which can lead to different exit vapour quality and then void fraction at a given heat and mass flux. Furthermore, the confinement effect and as a consequence the coalescence rate increases with decreasing channel width leading to large pressure drop. Jones and Garimella [21] and Jafari et al. [22] investigated the effect of surface roughness on the two-phase pressure drop and agreed that increasing the average surface roughness results in an increase in the two-phase pressure drop. This was attributed to the large wall shear stress induced by the activation of more nucleation sites on the rough surfaces. The effect of surface material may arise from the variations in surface microstructure induced by the material ductility/hardness which in turn affects the number of active nucleation sites and consequently the two-phase pressure drop as reported by Pike-Wilson and Karayiannis [23] for mini diameter tubes made of stainless steel, copper and brass and Al-Zaidi et al. [24] for microchannels made of aluminium and copper.

Although there is an agreement among most researchers on the effect of different parameters on the measured two-phase pressure drop, as presented above, there is still a wide scatter among the existing prediction models/correlations as will be discussed later. This may be attributed to the following reasons: (i) No single-phase validation performed in some experimental studies. Collecting two-phase pressure drop data without validating the single-phase pressure drop component in each studied geometry may result in a bias or large uncertainty in the measured two-phase pressure drop. If this set of data were used to develop a new correlation, then of course the correlation will also be affected by a possible large error in the data used. (ii) Most of the existing void fraction correlations, which is a key input parameter in all separated flow models, were based on adiabatic gas-liquid flow data in large diameter channels. A suitable void fraction model/correlation based on micro-scale data should be used with two-phase pressure drop models rather than the commonly used conventional void fraction correlations. (iii) Most of the existing correlations were suggested for the two-phase frictional pressure drop component. The experimental frictional component was deduced from the total measured pressure drop data by subtracting the acceleration and gravitational components, which depend strongly on the void fraction. In other words, these correlations may also be biased by the accuracy of the void fraction correlations. Accordingly, there is a need to test and evaluate the existing micro-scale pressure drop models/correlations using a wide range of experimental data. The aim of the current study is to evaluate the existing pressure drop models/correlations using a large experimental databank (four fluids; R134a, R245fa, HFE-7100 and HFE-7200, single and multi-channels configurations). A regression analysis was conducted at the end to correlate the experimental data since none of the assessed models/correlations predicted all the data with a reasonable accuracy. The assessed correlations/models are discussed in the next section.

2. Pressure drop models/correlations

Two-phase flow pressure drop in channels consists of three components: gravitational, acceleration and frictional components, as given by Eq. (1).

$$\Delta P_{tp} = \Delta P_g + \Delta P_{acc} + \Delta P_{fr} \tag{1}$$

These components can be calculated using two approaches, namely the homogeneous flow or the separated flow model. The following sections present a brief description for each approach in order to help clarify the differences among each model.

2.1. Homogeneous flow model

Both liquid and vapour phases are assumed to be mixed and flow at the same velocity. Therefore, the two-phase flow is considered as a single-phase flowing with the mixture properties averaged using the vapour quality. The homogeneous model is generally applicable for the bubbly flow or when the velocities of liquid and vapour are nearly the same. The three pressure drop components can be calculated using Eqs. (2–4), [25].

$$\Delta P_g = \frac{L_{tp} g * sin\theta}{v_{lg} x_o} ln\left[1 + x_o\left(\frac{v_{lg}}{v_l}\right)\right] \tag{2}$$

$$\Delta P_{acc} = G^2 v_{lg} x_o \tag{3}$$

$$\Delta P_{fr} = \frac{2 f_{tp} G^2 v_l L_{tp}}{D_h}\left[1 + \frac{x_o}{2}\left(\frac{v_{lg}}{v_l}\right)\right] \tag{4}$$

The specific volume difference v_{lg} is calculated by subtracting the specific volume of the saturated vapour from that of the saturated liquid, i.e. $v_{lg} = v_g - v_l$. The two-phase friction factor f_{tp} is calculated in the current study based on the channel geometry and flow regime (laminar or turbulent flow) as follows:

For laminar flow, $Re_{tp} < 2000$, the two-phase friction factor is calculated using Eq. (5) for circular channels and Eq. (6) for non-circular channels, Shah and London [26].

$$f_{tp} = \frac{16}{Re_{tp}} \tag{5}$$

$$f_{tp} = \left[24\left(1 - 1.355\beta + 1.946\beta^2 - 1.7012\beta^3 + 0.9564\beta^4 - 0.2537\beta^5\right)\right]/Re_{tp} \tag{6}$$

The parameter (β) is the channel aspect ratio, i.e. short (width or height)/long (width or height).

For turbulent flow, $2000 \le Re_{tp} < 20{,}000$, Blasius [27] was used for circular and non-circular channels:

$$f_{tp} = \frac{0.079}{Re_{tp}^{0.25}} \tag{7}$$

For $Re_{tp} \ge 20{,}000$, Eq. (8) is adopted for both channel geometries:

$$f_{tp} = \frac{0.046}{Re_{tp}^{0.2}} \tag{8}$$

The two-phase Reynolds number Re_{tp} can be calculated using Eq. (9).

$$Re_{tp} = GD_h/\mu_{tp} \tag{9}$$

where G, D_h and μ_{tp} are the channel mass flux, channel hydraulic diameter and two-phase mixture viscosity, respectively. A number of

Table 1
Two-phase mixture viscosity models for the homogeneous flow model.

Author(s)	Equation
McAdams et al. [50]	$\frac{1}{\mu_{tp}} = \frac{x_o}{\mu_g} + \frac{1-x_o}{\mu_l}$
Cicchitti et al. [51]	$\mu_{tp} = x_o\mu_g + (1-x_o)\mu_l$
Owens [52]	$\mu_{tp} = \mu_l$

models were proposed in literature to calculate the two-phase mixture viscosity, see Table 1. Some researchers, [28], recommended a fixed value of 0.003 for the two-phase friction factor f_{tp} based on data for flow boiling of water in horizontal rectangular multi-channels with channel dimensions of 0.23 × 0.71 mm.

2.2. Separated flow models

In these models, the liquid and vapour phases were assumed to flow separately with different velocities. The two-phase gravitational pressure drop component in Eq. (1) can be calculated using Eq. (10), [25].

$$\Delta P_g = \frac{L_{tp} g \sin\theta}{x_o} \int_0^{x_o} \left[\frac{\alpha}{v_g} + \frac{(1-\alpha)}{v_l}\right] dx \tag{10}$$

The two-phase acceleration pressure drop component is given by Eq. (11), [25].

$$\Delta P_{acc} = G^2 v_l \left[\frac{x_o^2}{\alpha_o}\left(\frac{v_g}{v_l}\right) + \frac{(1-x_o)^2}{1-\alpha_o} - 1\right] \tag{11}$$

In the above, α_o is the void fraction at the exit vapour quality. In literature, there are many models and correlations for the calculation of void fraction. In this paper, five widely used models/correlations are examined, as summarized in Table 2. It is worth noting that the correlation by Zivi [29] is widely used in literature. The two-phase frictional pressure drop component can be calculated using either Eq. (12) [30] or Eq. (13) [25].

$$\Delta P_{fr} = \frac{2L_{tp}G^2 v_l}{D_h}\frac{1}{x_o}\int_0^{x_o} \left[f_l (1-x)^2 \varnothing_l^2\right] dx \tag{12}$$

$$\Delta P_{fr} = \frac{2L_{tp}f_{lo}G^2 v_l}{D_h}\frac{1}{x_o}\int_0^{x_o} \left[\varnothing_{lo}^2\right] dx \tag{13}$$

where $\varnothing_l^2$ and $\varnothing_{lo}^2$ are the saturated liquid two-phase multiplier and the liquid only two-phase multiplier, respectively. The saturated liquid two-phase multiplier can be calculated from Eq. (14), [31].

$$\varnothing_l^2 = 1 + \frac{C}{X} + \frac{1}{X^2} \tag{14}$$

where C and X are the Martinelli–Chisholm constant and the Lockhart–Martinelli parameter, respectively. The Lockhart-Martinelli parameter depends on the flow regimes, i.e. laminar or turbulent. Table 3 summarizes the definition of the Lockhart-Martinelli parameter for the four different flow regimes, i.e. (1) laminar liquid-laminar vapour, (2) laminar liquid-turbulent vapour, (3) turbulent liquid-laminar vapour and (4) turbulent liquid-turbulent vapour. These regimes can be identified by calculating Re_{ls} and Re_{gs} using a threshold value of 2000 between laminar and turbulent flows. The superficial liquid and vapour Reynolds number Re_{ls} and Re_{gs} in Table 3 are calculated using Eq. (15) and (16), respectively.

$$Re_{ls} = G(1-x)D_h/\mu_l \tag{15}$$

$$Re_{gs} = GxD_h/\mu_g \tag{16}$$

The saturated liquid and vapour Fanning friction factor f_l and f_g in Table 3 can be calculated using Eqs. (5–8) based on the channel geometry and flow regime and replacing Re_{tp} with the superficial liquid and vapour Reynolds number Re_{ls} and Re_{gs} defined in Eqs. (15–16). The liquid only Fanning friction factor f_{lo} in Eq. (13) can be calculated using Eq. (5–8), but with the liquid only Reynolds number Re_{lo} instead of the Re_{tp}, i.e. $Re_{lo} = GD_h/\mu_l$, [25].

Several models/correlations were suggested by a number of researchers for the prediction of the two-phase flow pressure drop as summarized in Appendix I, which includes 26 models/correlations. The modifications of the original Lockhart-Martinelli model that were proposed by researchers are also summarized in Appendix I. These modifications included either correlating the Martinelli-Chisholm constant (C) or correlating the two-phase multiplier. For example, Mishima and Hibiki [32] correlated the Lokhart-Chisholm constant as a function of

Table 3
Lockhart–Martinelli parameter for different flow regimes, [30].

Flow regimes	Thresholds of Reynolds number	Equation
laminar liquid-laminar vapour	$Re_{ls} < 2000$ and $Re_{gs} < 2000$	$X_{ll} = \left(\frac{\mu_l}{\mu_g}\right)^{0.5}\left(\frac{1-x}{x}\right)^{0.5}\left(\frac{\rho_g}{\rho_l}\right)^{0.5}$
laminar liquid-turbulent vapour	$Re_{ls} < 2000$ and $Re_{gs} \geq 2000$	$X_{lt} = \left(\frac{f_l}{f_g}\right)^{0.5}\left(\frac{1-x}{x}\right)\left(\frac{\rho_g}{\rho_l}\right)^{0.5}$
turbulent liquid-laminar vapour	$Re_{ls} \geq 2000$ and $Re_{gs} < 2000$	$X_{tl} = \left(\frac{f_l}{f_g}\right)^{0.5}\left(\frac{1-x}{x}\right)\left(\frac{\rho_g}{\rho_l}\right)^{0.5}$
turbulent liquid-turbulent vapour	$Re_{ls} \geq 2000$ and $Re_{gs} \geq 2000$	$X_{tt} = \left(\frac{\mu_l}{\mu_g}\right)^{0.1}\left(\frac{1-x}{x}\right)^{0.9}\left(\frac{\rho_g}{\rho_l}\right)^{0.5}$

Table 2
Void fraction models and correlations.

Author(s)	Equation
Homogeneous model	$\alpha_o = \left[1 + \frac{1-x_o}{x_o}\left(\frac{\rho_g}{\rho_l}\right)\right]^{-1}$
Zivi [29]	$\alpha_o = \left[1 + \frac{1-x_o}{x_o}\left(\frac{\rho_g}{\rho_l}\right)^{0.67}\right]^{-1}$
Lockhart and Martinelli [30]	$\alpha_o = \left[1 + 0.28\left(\frac{1-x_o}{x_o}\right)^{0.64}\left(\frac{\rho_g}{\rho_l}\right)^{0.36}\left(\frac{\mu_l}{\mu_g}\right)^{0.07}\right]^{-1}$
Rouhani and Axelsson [53]	$\alpha_o = \frac{x_o}{\rho_g}\left[\{1+0.12(1-x_o)\}\left(\frac{x_o}{\rho_g} + \frac{1-x_o}{\rho_l}\right) + \frac{1.18(1-x_o)\{g\sigma(\rho_l-\rho_g)\}^{0.25}}{G\rho_l^{0.5}}\right]^{-1}$
Chisholm [54]	$\alpha_o = \left[1 + \left(\frac{1-x_o}{x_o}\right)\left(\frac{\rho_g}{\rho_l}\right)\sqrt{1 - x_o\left(1 - \frac{\rho_l}{\rho_g}\right)}\right]^{-1}$

hydraulic diameter only. Some other researchers such as Qu and Mudawar [28] and Lee and Garimella [1] included the mass flux as well as the hydraulic diameter. Most researchers used dimensionless groups such as Bond number, Froude number, Reynolds number, Weber number and Boiling number, see Appendix I, for all other dimensionless groups and the nomenclature section for definitions. The use of a wide range of dimensionless groups in literature to correlate the frictional two-phase pressure drop indicates that the interaction between the liquid and vapour phases is very complex in gas-liquid two-phase flow. Since there are two channel geometries (circular and non-circular channels), the heat flux required for the definition of the Boiling number used in some of the correlations summarized in Appendix I should be clarified here. It is well-known that the boiling number is defined as:

$$Bo = \frac{q_w''}{G i_{lg}} \tag{17}$$

where q_w'' and i_{lg} are the wall heat flux and the latent heat of vaporization, respectively. The wall heat flux is the heat flux at the wetted perimeter, i.e. channel bottom and side-walls. In multi-microchannels configurations, the channels are cut on the top surface of a large metal block and thus the wall heat flux is calculated from the heat flux at the base of the heat sink q'', which is obtained from the measured vertical temperature gradient and the 1D heat conduction equation. Fig. 1 illustrates the definition of the heat flux for single and multi-channels configurations. In single circular channels, the wall heat flux is defined as:

$$q_w'' = \frac{(IV - Q_{loss})}{\pi D_i L} \tag{18}$$

where I and V are the applied current and voltage, respectively and Q_{loss} is the heat loss. For rectangular channels, the wall heat flux can be calculated for the fully-heated channels (heated from all four sides) using Eq. (19) while Eq. (20) is used for the partially-heated channels (channels with adiabatic top side).

$$q_w'' = \left[\frac{W_b}{2N(H_{ch} + W_{ch})}\right] q'' \tag{19}$$

$$q_w'' = \left[\frac{W_b}{N(2H_{ch} + W_{ch})}\right] q'' \tag{20}$$

Fig. 2 depicts a comparison among pressure drop models that included circular passages (11 models), assuming a vertical tube with inner diameter 0.5 mm and 100 mm length, fluid R134a, mass flux of 200 kg/m^2 s and inlet pressure of 6 bar. This figure indicates that the two-phase pressure drop increases with increasing exit vapour quality for all correlations. However, a large disagreement among these correlations can clearly be seen, especially as the exit vapour quality increases. Therefore, the selection of an acceptable correlation poses a significant challenge in the thermal design of two-phase system.

The past correlations summarized in Appendix I were arranged in this paper according to three configurations, i.e. single channel, multi-channels and correlations covering both geometries. The validity range of each model is summarized in the last column of Appendix I. Generally, different parameters were introduced to calculate the Chisholm constant such as channel hydraulic diameter or aspect ratio, mass flux, Reynolds number, Lockhart–Martinelli parameter, Confinement number, Weber number and Boiling number. It is well known that different forces can affect the two-phase pressure drop components in conventional and micro-channels. The effect of gravitational and surface tension forces is included in the Bond number and Confinement number while inertia and viscous forces are included in the definition of the Reynolds and the inertia and surface tension forces are included in the Weber number. Some researchers used the Boiling number to include the effect of heat flux, mass flux and latent heat of vaporization.

3. Data-bank description

The existing data-bank of two-phase flow pressure drop was collected from several experimental investigations that were conducted by our research group, see Table 4. The total pressure drop along the channel was experimentally measured using differential pressure transducers. Because the flow enters the channel(s) with some degree of sub-cooling, a small part of the channel remains in the single-phase flow regime. Then the two-phase pressure drop was calculated by subtracting the single-phase pressure drop part from the total measured pressure drop as shown in Eq. (21). The single-phase pressure drop part was calculated from Eq. (22).

$$\Delta P_{tp} = \Delta P_{meas} - \Delta P_{sp} \tag{21}$$

$$\Delta P_{sp} = \frac{2fG^2 L_{sp}}{\rho_l D_h} \tag{22}$$

where f, G, L_{sp}, ρ_l and D_h are the friction factor, mass flux, single-phase length, liquid viscosity and channel diameter (hydraulic diameter), respectively. The single-phase length can be calculated from the energy balance between the liquid inlet temperature and the local saturation temperature at the end of the single-phase region, see [23]. Both vertical and horizontal test sections were examined at different operating conditions. All the measuring instruments were carefully calibrated and both degassing process and single-phase validation were carried out before conducting the two-phase flow boiling experiments. The repeatability of the two-phase flow results was also checked. In the experiments summarized in Table 4, all these essential steps are necessary to ensure high accuracy. One of our experimental test sections was described by Pike-Wilson and Karayiannis [23] and is shown in Fig. 3(a). The authors conducted two-phase flow boiling of R245fa in vertical tubes having 1.1 mm inner diameter and heated length of 300 mm. In

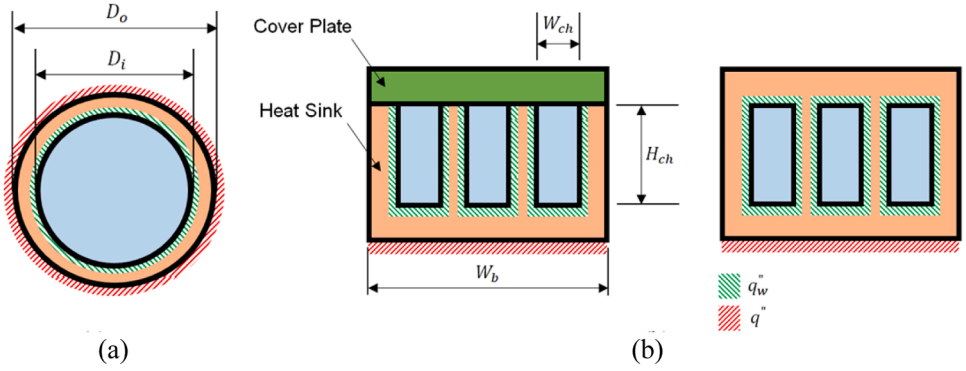

Fig. 1. Direct heat flux q_w'' and indirect heat flux q'' for different channel geometries: (a) Circular channel (b) Non-circular channel.

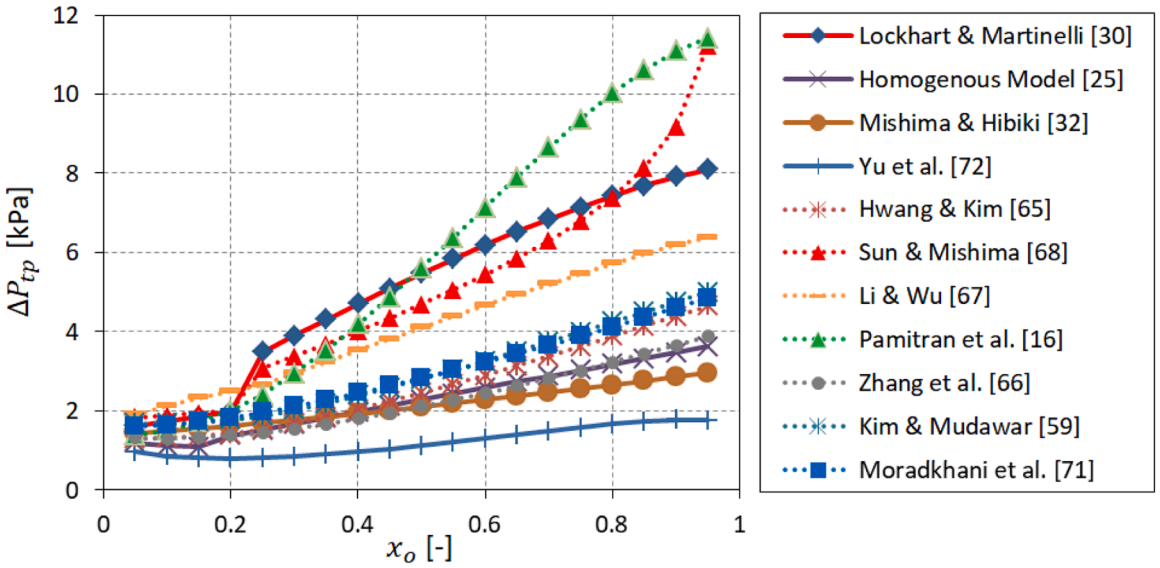

Fig. 2. Discrepancy in the existing correlations of two-phase pressure drop of R134a in 0.5 mm vertical tube of length 100 mm at mass flux of 200 kg/m^2 s and inlet pressure of 6 bar, using different existing correlations.

Table 4
Experimental operating conditions of the collected data (1612 data points).

Vertical upward flow in tubes: Author	Fluid	D_i [mm]	L [mm]	Metal	P_{sys} [bar]	G [kg/m^{2}s]	$q_w^{"}$ [kW/m^2]	Data Points
Al-Gaheeshi [35]	R245fa	1.1–2.01–2.88–4.26	150–210–300–500	SS	1.85–3	200–500	3 – 187	358
Pike-Wilson and Karayiannis [23]	R245fa	1.1	300	Cu-Br	1.8 – 2.5	100–400	4 – 38	179
Huo et al. [33]	R134a	2.01–4.26	213–500	SS	8 – 14	100–500	14–148	245
Shiferaw et al. [34]	R134a	1.1–2.88	150–300	SS	6 – 12	100–500	14–148	167
Mahmoud et al. [2]	R134a	0.52–1.1	100–150–300–450	SS	6 – 10	200–700	2 – 146	343

Horizontal flow in multi-channels: Author	Fluid	D_h [mm]	$H_{ch}/W_{ch}/L$ [mm]	N [-]	Metal	P_{sys} [bar]	G [kg/m^{2}s]	$q_w^{"}$ [kW/m^2]	Data Points
Al-Zaidi et al. [20]	HFE-7100	0.46	0.35/0.7/25 0.46/0.46/25 0.7/0.35/25	25 36 40	Cu–Al	1	50–250	10–192	269
Lee and Karayiannis [14]	HFE-7200	0.48	0.7/0.36/20	44	Cu	1 – 2	200–400	24–234	51

Dimensionless parameters: Parameter	Range
Superficial liquid Reynolds number	0.58–13,405
Superficial vapour Reynolds number	76.4 – 170,407
Boiling number	(0.024–8.21)× 10^{-3}
Prandtl number	3.15–7.62
Reduced pressure	0.044–0.34

Al: Aluminium.
Br: Brass.
Cu: Copper.
SS: Stainless steel.

this test section, a direct electric power was applied to the test section. A glass tube having the same inner diameter as the test section was also located at the exit of the test section to visualize flow patterns using Phantom high-speed camera. Lee and Karayiannis [14] conducted two-phase flow experiments using HFE-7200 as a working fluid in horizontal multi-channels. The heat sink was manufactured with a footprint area of 20 × 20 mm and four cartridge heaters were inserted from the bottom to supply the heat flux. In this design, forty-four rectangular and parallel microchannels were milled having a channel height of 0.7 mm, channel width of 0.36 mm and fin width of 0.11 mm. A transparent cover plate made of polycarbonate sheet was clamped on the top side as shown in Fig. 3(b) in order to capture the two-phase flow patterns. The test section included five main parts; top plate, cover plate, heat sink block, housing and bottom plate. An O-ring was placed inside a sealing groove between the cover plate and the heat sink to prevent any leakage. All these five parts were tightly assembled together using a set of long screws. Temperature and pressure measurements were conducted using thermocouples, pressure and differential pressure transducers.

Table 4 presents a summary of the experimental data-bank that includes single channel (tube) and multi-channels heat sink. Different working fluids were tested namely R134a, R245fa, HFE-7100 and HFE-7200 using channels with hydraulic diameter ranging from 0.46 to 4.26

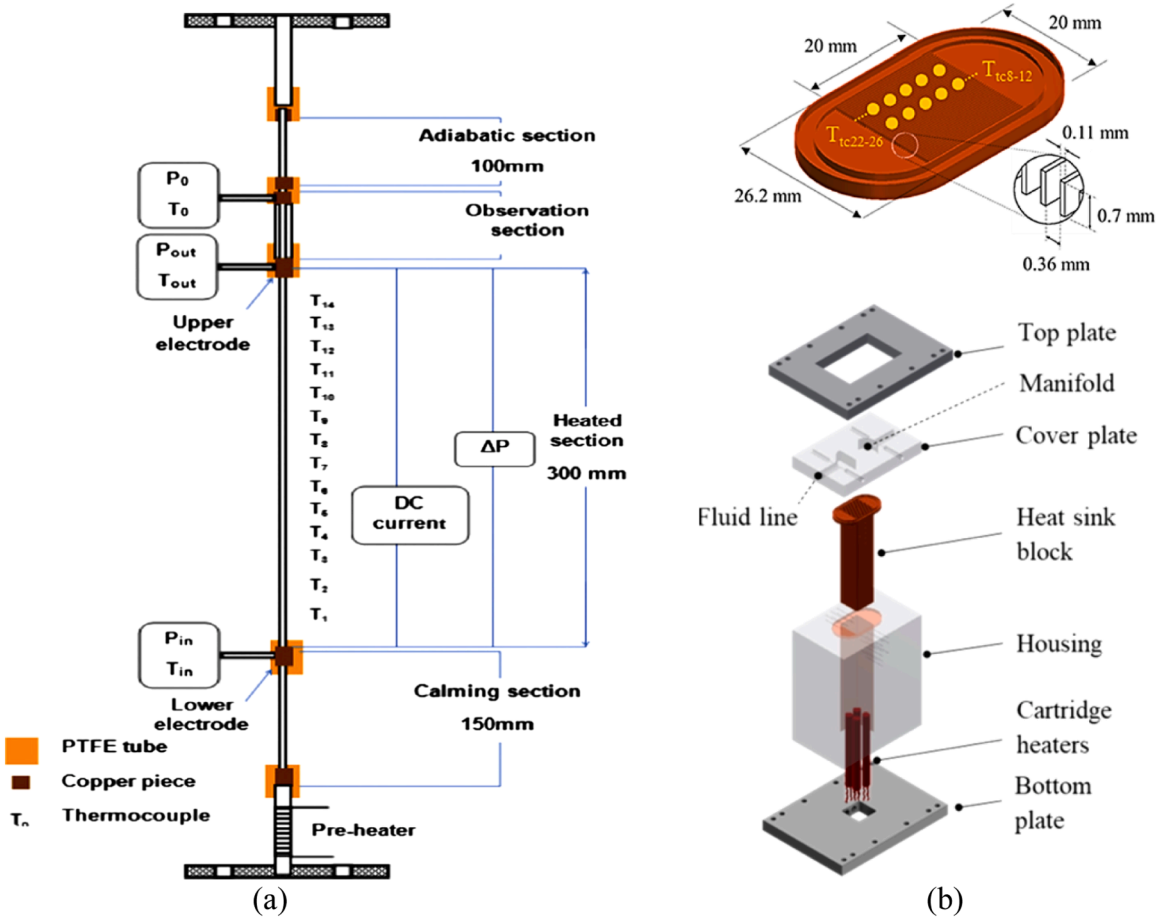

Fig. 3. Experimental test section: (a) Vertical tube, [23] (b) Horizontal multi-channels, [14].

mm and heated length of 20−500 mm. The collected data includes inlet pressure of 1 − 14 bar, inlet sub-cooling of about 2–5 K, mass flux of 50−700 kg/m^2 s, wall heat flux of 2 − 234 kW/m^2 and exit vapour quality up to one. Moreover, the databank includes channels made of different metals (copper, stainless steel, brass and aluminium). The uncertainty in the measurements of the total pressure drop in all the experimental data that we have used in this analysis was less than 0.42%, see references [2,14,20,23,33–35].

The single-phase pressure drop data points were excluded from the databank and 1612 data points of two-phase flow pressure drop were used for the evaluation of the existing models. Also, the data after the occurrence of dry out were also excluded from the databank as seen in Fig. 4 which shows the range of the experimental data plotted for R134a, as an example, in 1.1 mm stainless steel vertical tube at inlet pressure of 10 bar and mass flux of 500 kg/m^2 s. It also includes R245fa in a brass vertical tube of 1.1 mm inner diameter and 300 mm length at mass flux of 300 kg/m^2 s and system pressure of 1.8 bar. This figure indicates that the data used in the comparison was for exit vapour quality more than zero, i.e. the liquid single-phase region was not included. This figure also shows that the measured pressure drop increased with increasing vapour quality and the trend did not show a sudden drop at high exit quality (see yellow area), which was commonly reported in large diameter channels.

Table 4 also presents the experimental operating conditions and the dimensionless parameters that are covered by the data-bank. The superficial liquid Reynolds number Re_{ls} covers the range 0.58−13,405 and the superficial vapour Reynolds number Re_{gs} is between 76.4 and 170,407. The Boiling number is in the range of 0.024−8.21×10^{-3} and the liquid Prandtl number covers the range 3.15−7.62. Finally, the reduced pressure ($RP = P_i/P_{cr}$) covered in the data-bank ranges from

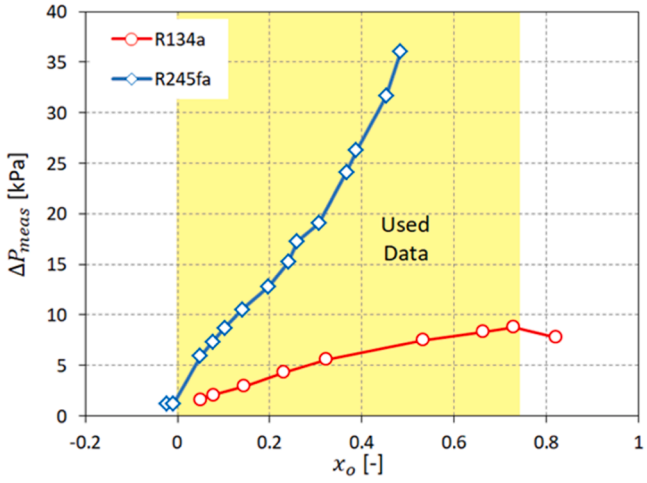

Fig. 4. Experimental measured pressure drop versus exit vapour quality for: R134a in a stainless steel vertical tube of 1.1 mm inner diameter and 150 mm length at mass flux of 500 kg/m^2 s and system pressure of 10 bar. R245fa in a brass vertical tube of 1.1 mm inner diameter and 300 mm length at mass flux of 300 kg/m^2 s and system pressure of 1.8 bar.

0.044 to 0.34.

Fig. 5(a) depicts the distribution of all data points based on the diameter and indicates that 26.5 % of the data are for channels with diameter less than 1 mm, 33.8 % of the data are for the 1.1 mm diameter channel and 39.7 % of the data are for channels with diameter larger

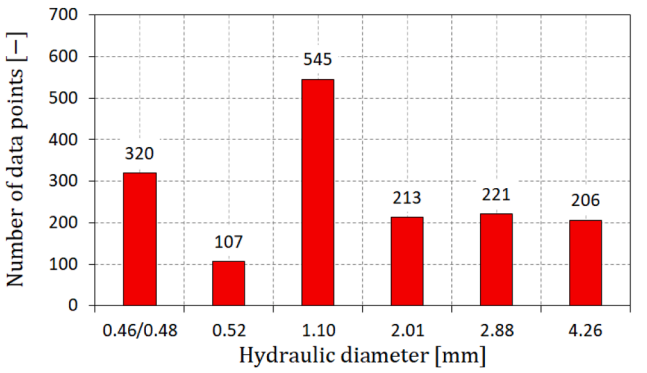

(a)

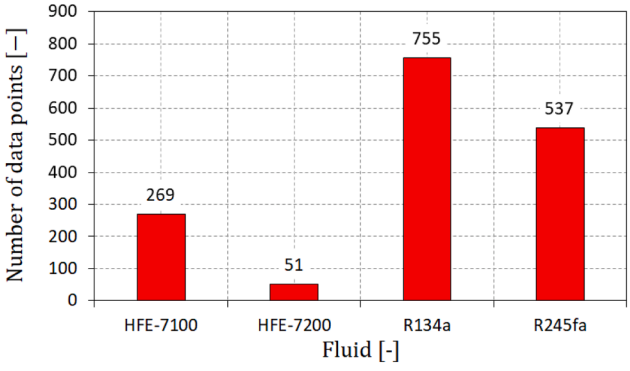

(b)

Fig. 5. Distribution of the data points for different parameters.

than 1 mm (2.01–4.26 mm). Based on the fluid, Fig. 5(b) shows that the collected data points are 755 (46.8 %), 537 (33.3 %), 269 (16.7 %) and 51 (3.1 %) for R134a, R245fa, HFE-7100 and HFE-7200, respectively. The distribution of the flow regimes (laminar/turbulent) is plotted in Fig. 6 based on the superficial liquid Reynolds number Re_{ls} and the superficial vapour Reynolds number Re_{gs}. Four flow regimes can be identified based on the thresholds of Reynolds number presented in Table 3. The figure shows that 63.2 % of all data points are located in the laminar liquid-turbulent vapour (*lt*), 22.6 % are within the turbulent liquid-laminar vapour (*tt*) and 14 % are in the laminar liquid-laminar vapour (*ll*). The turbulent liquid-laminar vapour regime (*tl*) shows only 0.2 %. The figure also shows that all the data points of channel diameter of

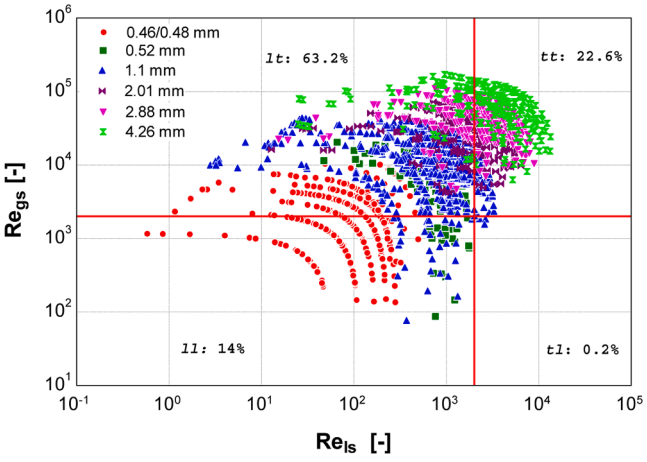

Fig. 6. Distribution of superficial liquid Reynolds number Re_{ls} and superficial vapour Reynolds number Re_{gs} of all data points (*ll*: laminar liquid-laminar vapour, *lt*: laminar liquid-turbulent vapour, *tl*: turbulent liquid-laminar vapour, *tt*: turbulent liquid-turbulent vapour).

2.01, 2.88 and 4.26 mm are within the turbulent vapour regime while the data points of the smaller diameter ranges, i.e. 0.46, 0.48, 0.52 and 1.1 mm, fall in both the laminar and the turbulent vapour regimes.

The collected data were compared with the models and correlations summarized in Appendix I, which were developed for conventional, macro and micro-scale channels. Therefore, the threshold diameter segregating macro and micro-scale passages should be agreed first. Two approaches were adopted by researchers in the literature, namely the simple geometrical approach (fluid independent) and the bubble confinement approach (fluid-dependent). The physical channel size is used in the geometrical approach. This includes surface area density (ζ, ratio of heat transfer area to unit volume) and channel inner diameter or hydraulic diameter. Shah and Sekulić [36] gave the following criteria for different scales using the surface area density:

$\zeta \geq 15{,}000\ m^2/m^3$ for micro-scale.
$\zeta \geq 3000\ m^2/m^3$ for meso-scale (macro or mini).
$\zeta \geq 700\ m^2/m^3$ for large scale.

Kandlikar and Grande [37] used the channel hydraulic diameter to classify these scales as follows:

$0.01 < D_h \leq 0.2$ mm for micro-scale.
$0.2 < D_h \leq 3$ mm for mini-scale.
$D_h > 3$ mm for conventional scale.

The dominant gravitational and surface tension forces are considered in the bubble confinement approach. In this approach the fluid properties are used and presented in dimensionless parameters. Table 5 presents the different criteria suggested by researchers to define macro to micro-scale transition as summarised in Karayiannis and Mahmoud [38]. It is worth mentioning that the criterion given by each researcher was re-written by [38] as a function of Laplace number, *La*, for the sake of comparison. Further discussion about each criterion can be found in [38]. Fig. 7 shows the threshold diameter between macro and micro-scale calculated, using the criteria summarized in Table 5, at $P = 1$ bar and $G = 200$ kg/m^2 s using four different fluids (HFE-7100, HFE-7200, R-134a, R-245fa), which were included in our experimental databank. It can be seen that, for a given fluid, the predicted threshold value varies significantly among these criteria. For example, for HFE-7100, the threshold diameter predicted by Harrichian and Garimela [39] is 0.51 mm, while its significantly higher using the criterion by given Brauner and Maron [40], which gives a value of 5.23 mm. This figure also shows that, for a given criterion, the threshold diameter is not the same when different fluids are used due to their different thermophysical properties. The present authors believe that this transition from macro to micro-scale is a gradual one and hence there is a difficulty in obtaining a precise definition, which must include the fluid properties, see [38]. It seems that the transition is from macro to small and then micro-scale and further work may be needed to fully clarify this. In our experimental databank, the tube diameter and channel hydraulic diameter is in the range 0.46 to 4.26 mm and based on the above discussion, confinement effects are important and hence reference can be

Table 5
Different criteria to define macro to micro-scale, [38].

Authors	Criterion
Brauner and Moalem-Maron [40]	$D = 2\pi La$
Kew and Cornwell [60]	$D = \pi La$
Triplett et al. [61]	$D = La$
Ullman and Brauner [62]	$D = \sqrt{1.6}La$
Harirchian and Garimella [39]	$D = \sqrt{(160\mu La)/G}$
Ong and Thome [63]	$D = 2.94La$
Tibiriçá, and Ribatski [64] _c1	$D = La\sqrt{8cos\theta}$
Tibiriçá, and Ribatski [64] _c2	$D = La\sqrt{1/20}$

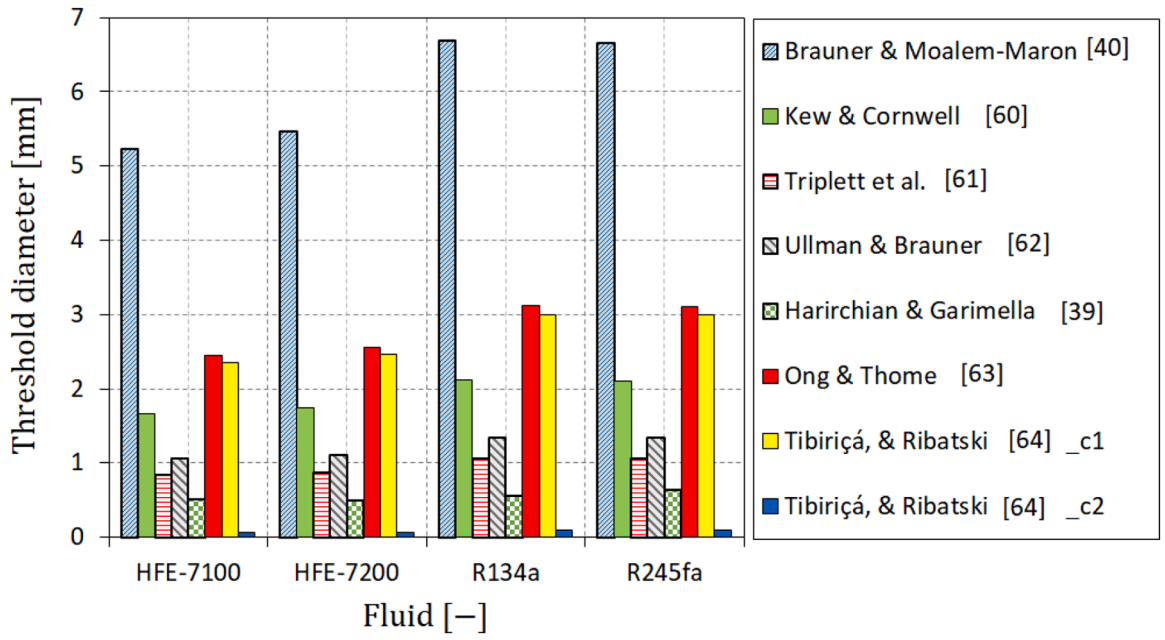

Fig. 7. Threshold diameter between macro and micro transition for different fluids and criteria.

made to flow boiling in small to micro-scale passages.

4. Data comparison

In this analysis, 1612 data points were compared with the correlations summarized in Appendix I. Most of these correlations are well-known and widely used by the research community. They were proposed for different working fluids, operating conditions and channel size/geometries. The statistical assessment was conducted based on the percentage of data points predicted within the ±30 % error bands (θ) defined in Eq. (23) and the mean absolute error (MAE) percentage defined in Eq. (24).

Table 6
Comparison with the existing models and correlations for calculating two-phase pressure drop. The prediction of some correlations was improved by changing the equations for calculating μ_{tp}, α, X and f, as shown in brackets.

Author(s)/Model	Two-phase Mixture Viscosity (μ_{tp})	Void Fraction (α)	Lockhart–Martinelli Parameter (X)	Fanning Friction Factor (f)	MAE (improved)
HFM	McAdams et al. [50] ($f_{tp} = 0.003$)	–	–	Eq. (5–8)	53 % (46 %)
Raju et al. [55]	–	Homogeneous Model (Lockhart & Martinelli)	X_{lt} or X_{tl} (refer to Table 3)	$f_k = \frac{3.119}{Re_{ks}^{0.55}}$	60 % (51 %)
Choi et al. [47]	–	Zivi [29] (Lockhart & Martinelli)	X_{tt} (refer to Table 3)	Eq. (5–8) using Re_{ls} & Re_{gs}	>100 % (73 %)
Markal et al. [56]	–	Zivi [29] (Lockhart & Martinelli)	X_{lt} or X_{tl} (refer to Table 3)	As above	73 % (62 %)
Mishima & Hibiki [32]	–	Lockhart & Martinelli [30]	X_{ll}	As above	52 %
Li & Hibiki [49]	McAdams et al. [50]	As above	X_{lt} or X_{tl}	As above	51 %
Lockhart & Martinelli [30]	–	As above	As above	As above	68 %
Hwang & Kim [65]	–	As above	As above	As above	80 %
Warrier et al. [45]	–	As above	As above	As above	>100 %
Zhang et al. [66]	–	As above	As above	As above	56 %
Li & Wu [67]	–	As above	As above	As above	67 %
Pamitran et al. [16]	–	Rouhani & Axelsson [53]	As above	As above	>100 %
Sun & Mishima [68]	–	Zivi [29]	As above	As above	66 %
Zeng et al. [44]	–	As above	As above	As above	>100 %
Lee & Lee [69]	–	As above	As above	As above	74 %
Lee et al. [48]	–	As above	As above	As above	>100 %
Keepaiboon et al. [46]	–	As above	As above	As above	>100 %
Huang & Thome [42]	–	As above	As above	As above	50 %
Lee & Mudawar [70]	–	As above	As above	As above	85 %
Huang et al. [41]	–	As above	As above	As above	47 %
Kim & Mudawar [59]	–	As above	As above	As above	76 %
Qu & Mudawar [28]	–	As above	X_{ll}	As above	55 %
Lee & Garimella [1]	–	As above	As above	As above	>100 %
Moradkhani et al. [71]	–	As above	–	As above	51 %
Yu et al. [72]	–	As above	$18.65\left(\frac{Re_{gs}^{0.1}}{Re_{ls}^{0.5}}\right)\left(\frac{1-x}{x}\right)\left(\frac{\rho_g}{\rho_l}\right)^{0.5}$	As above	52 %
Zhang & Webb [43]	–	As above	–	Eq. (5–8) using Re_{lo} & Re_{go}	>100 %

– No equation required.

$$\theta = \frac{N_{pred}}{N_{exp}} 100\% \tag{23}$$

$$MAE = \frac{1}{N} \sum \left| \frac{\Delta P_{pred} - \Delta P_{exp}}{\Delta P_{exp}} \right| 100\% \tag{24}$$

where N is the total number of data points, ΔP_{pred} is the predicted two-phase pressure drop, and ΔP_{exp} is the experimental two-phase pressure drop.

Table 6 shows that the correlations by Huang et al. [41] and Huang and Thome [42] provided the smallest MAE of 47 % and 50 %, respectively. This comparison also shows that the homogeneous flow model had a MAE of 53 %. The mean absolute error was found to be greater than 100% using the correlations by Lee and Garimella [1], Pamitran et al. [16], Zhang and Webb [43], Zeng et al. [44], Warrier et al. [45], Keepaiboon et al. [46], Choi et al. [47] and Lee et al. [48].

It is worth mentioning that the accuracy of a correlation could be affected by the following parameters: two-phase mixture viscosity μ_{tp}, void fraction α, Lockhart–Martinelli parameter X and Fanning friction factors f. Therefore, the sensitivity of each correlation to the different available equations of calculating μ_{tp}, α, X and f was also carried out in this paper. In the discussion that flows we included only the cases where notable improvements in the predictive comparison with our data were possible when we varied the method of calculation of the above parameters.

4.1. Two-phase mixture viscosity

It is well-known that the two-phase mixture viscosity is used in the homogeneous flow model. Some separated flow models include the two-phase mixture viscosity such as the model given by Li and Hibiki [49]. Therefore, three different equations for calculating μ_{tp} (see Table 1) were evaluated. It was found that the homogeneous flow model strongly depends on the model used to calculate the mixture viscosity. The mean absolute error was found to be 53 %, 82 % and 122 % for the models by McAdams et al. [50], Cicchitti et al. [51] and Owens [52], respectively. When the three different equations of μ_{tp} were evaluated in the separated flow model by Li and Hibiki [49], the effect of different viscosity models was insignificant, i.e. MAE varied from 48 % to 51 %.

4.2. Void fraction

In literature, there are many equations that were developed and proposed for calculating void fraction. In this paper, five well-known equations are evaluated, see Table 2. Generally, the void fraction models by Zivi [29], Lockhart and Martinelli [30], Rouhani and Axelsson [53] and Chisholm [54] showed nearly similar results. However, the model by Lockhart and Martinelli [30] provided the smallest MAE when used in the correlation of Raju et al. [55] instead of the homogeneous model and in the correlations of Choi et al. [47] and Markal et al. [56] instead of the Zivi model [29], see Table. 6.

4.3. Lockhart-Martinelli parameter

The Lockhart-Martinelli parameter X can be calculated for four flow regimes namely laminar liquid-laminar vapour, laminar liquid-turbulent vapour, turbulent liquid-laminar vapour and turbulent liquid-turbulent vapour, see Table 3. Some authors recommended that the Lockhart-Martinelli parameter of a specific flow regime should be used with their correlations. We evaluated the comparative predictive results to variations due to the calculation based on the different flow regimes and found the effect to be insignificant in the present study. However, we recommend that this parameter should still be calculated based on the experimental flow regimes. It represents the ratio between the liquid and vapour friction factor, density and viscosity, which depends on the flow regimes.

4.4. Two-phase and single-phase friction factor

We examined the effect of the different methods of calculating the two-phase friction factor as used in the homogeneous model. The MAE was improved from 53 % when using Eq. (5−8) to 46 % when using the value recommended by Qu and Mudawar [28], as shown in Table 6.

The single-phase Fanning friction factor is used in most existing correlations, i.e. in the frictional pressure drop component and the Lockhart–Martinelli parameter. The Fanning friction factor for saturated liquid f_l, saturated vapour f_g and liquid only f_{lo} can be identified, as discussed in Section 2. It is well-known that, for laminar flow, Eq. (5) is used for circular channels, while Eq. (6) is adopted for non-circular channels. For turbulent flow in both channel geometries, this friction factor can be calculated using Eq. (7−8). However, the turbulent Fanning friction factor can be calculated using other equations. Eq. (25) was proposed by Petukhov et al. [57] for circular channels within the range $3000 \leq Re \leq 5 \times 10^6$.

$$f = (1.58ln(Re) - 3.28)^{-2} \tag{25}$$

Phillips [58] developed two correlations for circular channels, see Eq. (26), and non-circular channels as shown in Eq. (27−28).

$$f = \left(0.0929 + \frac{1.01612D}{L}\right) Re^{\left(-0.268 \; - \; \frac{0.3193D}{L}\right)} \tag{26}$$

$$f = \left(0.0929 + \frac{1.01612D_h}{L}\right) Re^{*\left(-0.268 \; - \; \frac{0.3193D_h}{L}\right)} \tag{27}$$

$$Re^* = Re\left[\left(\frac{2}{3} + \frac{11}{24}\right)\beta(2-\beta)\right] \tag{28}$$

We examined any possible improvement for each correlation to different equations for calculating the turbulent friction factor. There was no noticeable changes although Blasius [27] had the smallest MAE.

As shown in Table 6, the mean absolute error of all correlations even with the attempt of the present authors to improve by selecting the abovementioned equations of μ_{tp}, α, X and f was still large, i.e. the smallest MAE was 46 % and 47 %, see Fig. 8. It is interesting to note that the HFM showed a small MAE compared to other separated flow correlations. It is well known that the HFM assumes that the slip ratio of the two phases is one. This could indicate that the liquid and vapour velocities were the same, during the current data-points. This model is also applicable for the bubbly flow that was observed in our experimental results.

Since the total two-phase pressure drop in multi-channels could differ from that in single tubes, the data points of horizontal rectangular multi-channel heat sinks were then separated and compared with these correlations. It can be seen from Fig. 9 that the correlations by Qu and Mudawar [28] and Keepaiboon et al. [46] provided the smallest MAE of 28 % and 22 %, respectively. The homogeneous flow model also predicted the results well with a MAE of 28.6 %. This reasonable agreement by [28] and [46] could be due to the fact that these correlations were proposed for micro-scale horizontal rectangular multi-channels having micro-scales. It is worth mentioning that these two correlations showed a large disagreement when all the data-bank (including vertical tubes and multi-channels) was used. The success of the homogeneous model in multi-channels compared to all data-bank could be due to the good mixing between liquid and vapour phases.

The discrepancy between the present data-bank and the existing correlations could be due to the different working fluids, operating conditions, channel geometry/size/orientation, surface material/microstructures, single or multi-channels and heating process (adiabatic or flow boiling) that lead to different two-phase pressure drop ranges. For example, Fig. 10 depicts the comparison between the experimental data points and the correlation by Kim and Mudawar [59]. These data points

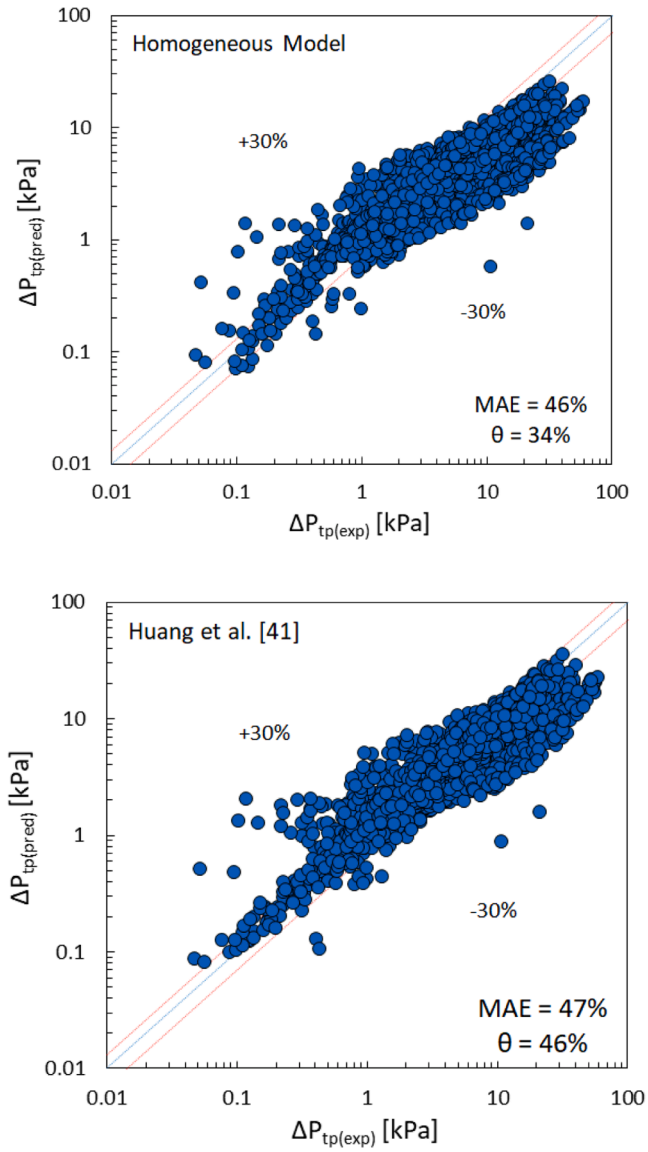

Fig. 8. Two-phase pressure drop comparison using all the data-bank (showing smallest MAE).

included flow boiling of HFE-7200 in horizontal rectangular multi-channels having 0.48 mm hydraulic diameter. It also covered high inlet sub-cooling data points, i.e. 20 K. Fig. 10(a) shows that this correlation predicted only 61 % of the data with a MAE of 53 %. It is clear from this figure that the data points of high inlet sub-cooling were over predicted by their correlation. This high inlet sub-cooling provided lower two-phase pressure drop due to the delay in flow transitions, i.e. small void fraction, [14]. When these low pressured drop data points were excluded from this comparison, a good agreement was found as shown in Fig. 10(b). The mean absolute error was reduced from 53 % to 24 % using this correlation.

5. Proposed correlation

The previous comparison showed that the smallest mean absolute error of 46 % was provided by the existing correlations using all the data points. In order to enhance the predictive capability for all data-bank, a regression analysis was applied on the present experimental data points. The separated flow method was used to propose a new correlation by calculating the experimental liquid only two-phase multiplier $\varnothing_{lo}^2$. This multiplier and all dimensional and non-dimensional parameters were

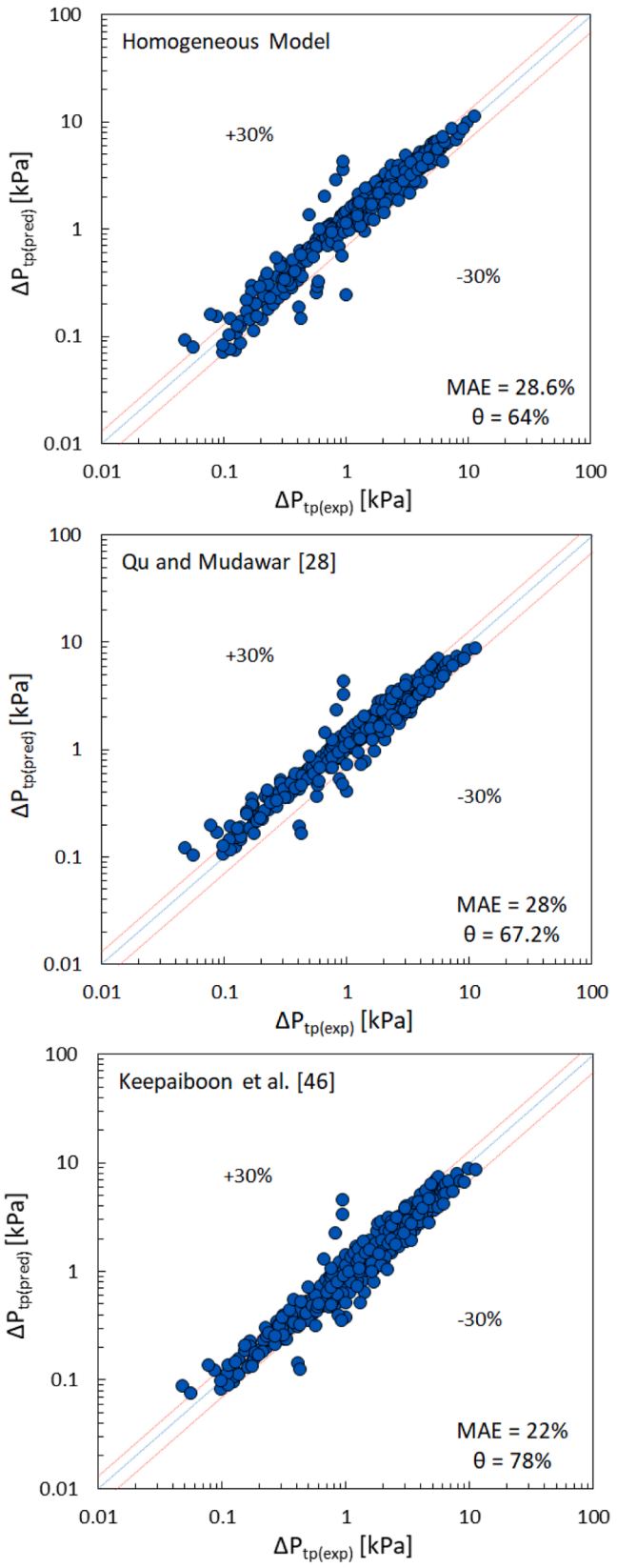

Fig. 9. Two-phase pressure drop comparison using the data-bank of multi-channels (showing smallest MAE).

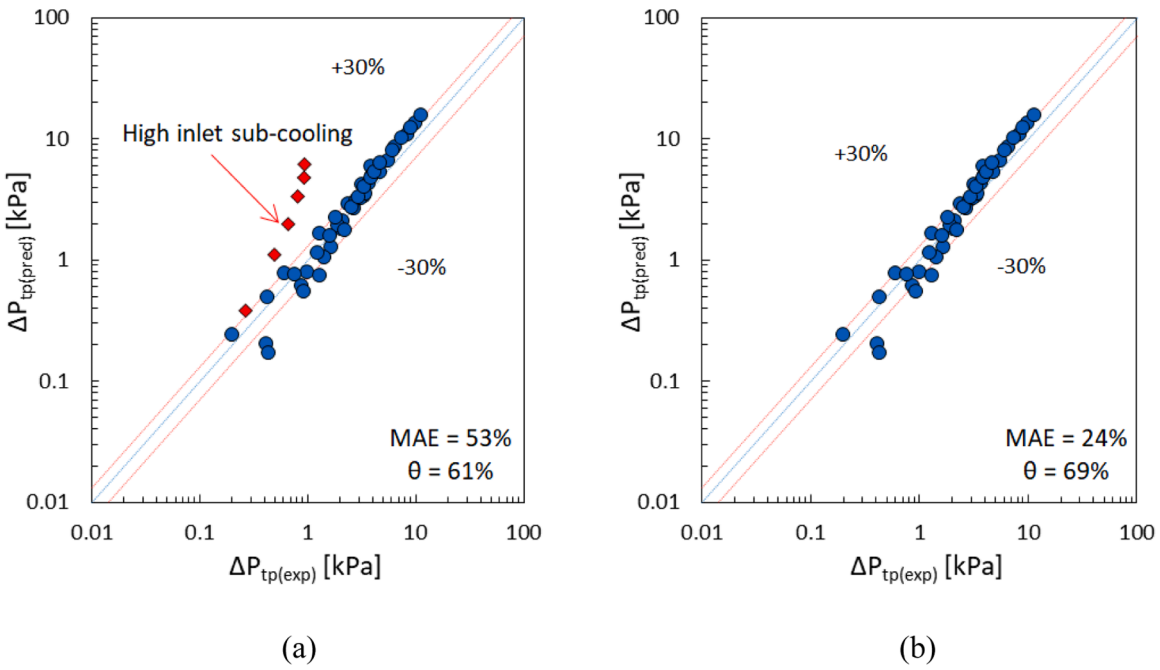

Fig. 10. Two-phase pressure drop comparison with the correlation by Kim and Mudawar [59] for HFE-7200 in horizontal rectangular multi-channels with 0.48 mm hydraulic diameter: (a) With high inlet sub-cooling data points (b) Without high inlet sub-cooling data points.

then examined to identify the best agreement. These parameters included (1-*x*), *Bd*, *RP*, *Co*, *Bo*, Re_{lo}, Re_{go}, Re_{ls}, Re_{gs}, We_{lo}, We_{go}, We_{ls}, We_{gs}, Su_{lo}, Su_{go}, *Fr*, *DR* and *X*. According to the discussion in Section 4, this regression analysis was carried out based on the following recommendations:

- The void fraction correlation by Lockhart and Martinelli [30] was adopted.
- The Lockhart-Martinelli parameter was calculated according to the experimental flow ranges at the threshold of Reynolds number of 2000, see Table 3.
- For laminar Fanning friction factor, the laminar theory for tubes and the correlation by Shah and London [26] for non-circular channels were used. For turbulent Fanning friction factor, the correlations by Blasius [27] were chosen.

Moreover, the data-bank was then separated into multi-channels and tubes according to the flow regimes as follows:

1. For rectangular multi-channels: laminar liquid-laminar vapour (*ll*) and laminar liquid-turbulent vapour (*lt*).
2. For circular single channels: laminar liquid-laminar vapour (*ll*), laminar liquid-turbulent vapour (*lt*), turbulent liquid-laminar vapour (*tl*) and turbulent liquid-turbulent vapour (*tt*).

It was found that the Boiling number *Bo* and the Lockhart–Martinelli parameter *X* have the strongest effect on the experimental frictional pressure drop component. This was also found for all flow regimes including the turbulent liquid-turbulent vapour regime as shown in Fig. 11. It is well-known that the Boiling number represents the influence of heat flux and mass flux, while the Lockhart–Martinelli parameter was utilized to characterize the effect of vapour quality, density ratio and viscosity ratio on two-phase pressure drop. These parameters have a significant effect on the flow boiling pressure drop during the present data points. Furthermore, the reduced pressure and the superficial vapour Reynolds number were included in this new correlation. These two dimensionless parameters take into account the influence of fluid properties, viscous and inertia forces. It is expected that the Boiling number has a significant effect at low mass fluxes, i.e. during the region where surface tension force dominates. At high mass flux, annular flow was the prevalent flow pattern when the inertia force could be the dominant force. The liquid only two-phase multiplier was then proposed as follows:

$$\varnothing_{lo}^2 = E\left(Bo^a X^b Re_{gs}^c RP^d\right) \tag{29}$$

The dimensionless number *E*, the experimental exponents (a, b, c, d) and all other conditions are summarized in Table 7. This new correlation was compared with the data points for each flow regime as shown in Fig. 12. The figure depicts that the proposed correlation predicted all the experimental data points of laminar liquid-laminar vapour regime with a MAE of 17 %. This figure also showed a reasonable prediction of all data points of both laminar liquid-turbulent vapour regime and turbulent liquid-laminar vapour regimes with a mean absolute error of 22 %. For turbulent liquid-turbulent vapour regime, this correlation predicted 84 % of data with a MAE of 18 %. When this correlation was used to evaluate all the data-bank, 77 % of all experimental data points were predicted by this correlation with a MAE of 20 %. It is worth mentioning that the six data points of high inlet sub-cooling (20 K) were still over predicted by this new correlation. Therefore, more experimental investigations are required to cover these operating conditions, i.e. high inlet sub-cooling, in order to improve the prediction. The comparative graph of multi-channels and tubes were also plotted separately using this correlation as shown in Fig. 13. Fig. 13(a) shows a MAE of 5 % between the proposed correlation and the data points of horizontal rectangular multi-channels using HFE-7100 in 0.46 mm hydraulic diameter at a system pressure of 1 bar, mass flux of 250 kg/m^2 s and exit vapour quality up to 0.92. Furthermore, a MAE of 10 % was found between this new correlation and the data points of vertical tubes using R245fa in 2.88 mm inner diameter, system pressure of 1.8 bar, mass flux of 400 kg/m^2 s and exit vapour quality up to 0.78, see Fig. 13(b). These two sets of data were selected, as examples, to show the predicted trend by the current correlation covering low and high vapour quality regions. The new correlation was proposed based on the current experimental data-bank that covered the following ranges:

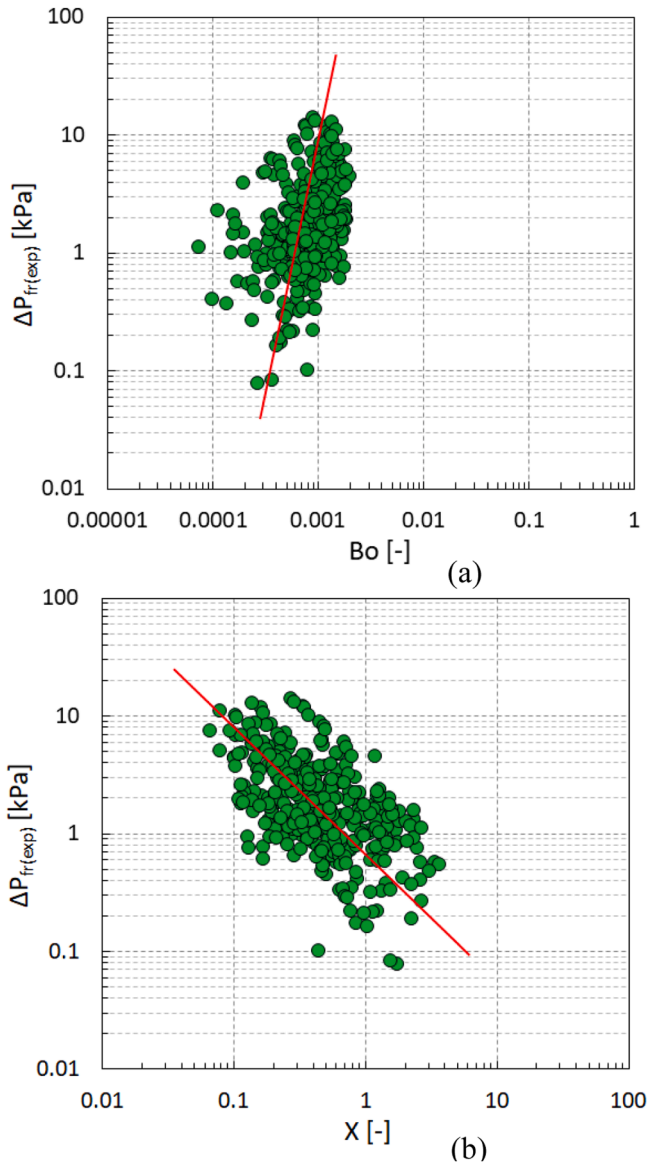

Fig. 11. Experimental frictional pressure drop for turbulent liquid-turbulent vapour regime versus: (a) Boiling number (b) Lockhart–Martinelli parameter.

Channel configuration: rectangular multi-channels and single circular channels.
Flow direction: horizontal and vertical upward flow.
Flow regime: for multi-channels: (*ll*) and (*lt*). For circular channels: (*ll*), (*lt*), (*tl*) and (*tt*).
Working fluid: R134a, R245fa, HFE-7100 and HFE-7200.
Hydraulic diameter: 0.46−4.26 mm.
Aspect ratio: 0.5 − 2.
Inlet pressure: 1 − 14 bar.
Mass flux: 50−700 kg/m^2 s.
Wall heat flux: 2 − 234 kW/m^2.
Exit vapour quality: $0 < x < 1$.
Superficial liquid Reynolds number: 0.58−13,405.
Superficial vapour Reynolds number: 76.4 − 170,407.
Boiling number: $(0.024–8.21) \times 10^{-3}$.
Prandtl number: 3.15−7.62.
Reduced pressure: 0.044−0.34.

Table 7
New correlation for calculating flow boiling pressure drop in horizontal rectangular multi-channels and vertical circular tubes.

Use Eq. (10) for calculating gravitational pressure drop component.
Use Eq. (11) for calculating acceleration pressure drop component.
Use Eq. (13) for calculating frictional pressure drop component.
Use the correlation by Lockhart and Martinelli [30] for calculating void fraction.
See Table 3 for calculating the Lockhart–Martinelli parameter.
The proposed liquid only two-phase multiplier is found as follows:
$\varnothing_{lo}^2 = E(Bo^a X^b Re_{gs}^c RP^d)$

Channel geometry and flow regime	E	a	b	c	d
Horizontal rectangular multi-channels:					
$Re_{ls} < 2000$ and $Re_{gs} < 2000$ (*ll*):	0.65	−0.6	−0.45	0.55	2.08
$Re_{ls} < 2000$ and $Re_{gs} \geq 2000$ (*lt*):	4.3×10^{-6}	−1.63	−0.16	1.2	1.72
Vertical circular channels:					
$Re_{ls} < 2000$ and $Re_{gs} < 2000$ (*ll*):	5×10^{12}	2.5	−0.2	−2	2
$Re_{ls} < 2000$ and $Re_{gs} \geq 2000$ (*lt*) or $Re_{ls} \geq 2000$ and $Re_{gs} < 2000$ (*tl*):	7×10^3 $We_{gs}^{0.67}$	0.45	0.085	−0.8	−0.7
$Re_{ls} \geq 2000$ and $Re_{gs} \geq 2000$ (*tt*):	7.6×10^5	1.1	−0.3	−0.47	−0.35

The friction factor is calculated based on the threshold Reynolds number of 2000 at exit quality as follows:
For laminar flow $Re_{ks} < 2000$ in circular channels:
$f_k = \frac{16}{Re_{ks}}$
For laminar flow $Re_{ks} < 2000$ in rectangular channels, [26]:
$f_k = (24(1 - 1.355\beta + 1.946\beta^2 - 1.7012\beta^3 + 0.9564\beta^4 - 0.2537\beta^5))/Re_{ks}$
For turbulent flow $2000 \leq Re_{ks} < 20{,}000$ in both channel geometries, [27]:
$f_k = \frac{0.079}{Re_{ks}^{0.25}}$
For turbulent flow $Re_{ks} \geq 20{,}000$ in both channel geometries, [27]:
$f_k = \frac{0.046}{Re_{ks}^{0.2}}$
where k refers to l for saturated liquid or g for saturated vapour. β = *short*/*long*.
This correlation based on experimental data-bank including:
Fluids: R134a, R245fa, HFE-7100 and HFE-7200.
Hydraulic diameter: 0.46−4.26 mm.
Aspect ratio: 0.5 − 2.
Mass flux: 50−700 kg/m^2 s.
Inlet pressure: 1 − 14 bar.
Wall heat flux: 2 − 234 kW/m^2.
Vapour quality: $0 < x < 1$.

6. Conclusion

This paper presented a discussion on the assessment of existing models and correlations for calculating two-phase pressure drop in conventional and micro-scale channels. An experimental data-bank was used to evaluate these models and correlations that covered small/micro-scale, vertical/horizontal flow, single/multi-channels, different working fluids and surface substrates. A wide range of different operating conditions were included in this assessment. The main conclusions can be summarised as follows:

1. The evaluation of existing models and correlations showed that there was a large discrepancy among them. Different operating conditions, fluid properties, channel configurations and sizes could lead to different dominant parameters.
2. Further work may be needed to fully clarify the transition from macro to small and then micro-scale. This paper showed that, although many criteria were proposed to define these scales, there was no a general criterion that can be used to distinguish between macro and micro-scale.
3. The homogeneous flow model highly depended on the mixture viscosity model or the two-phase friction factor. The viscosity model by McAdams et al. [50] or the two-phase friction factor (0.003)

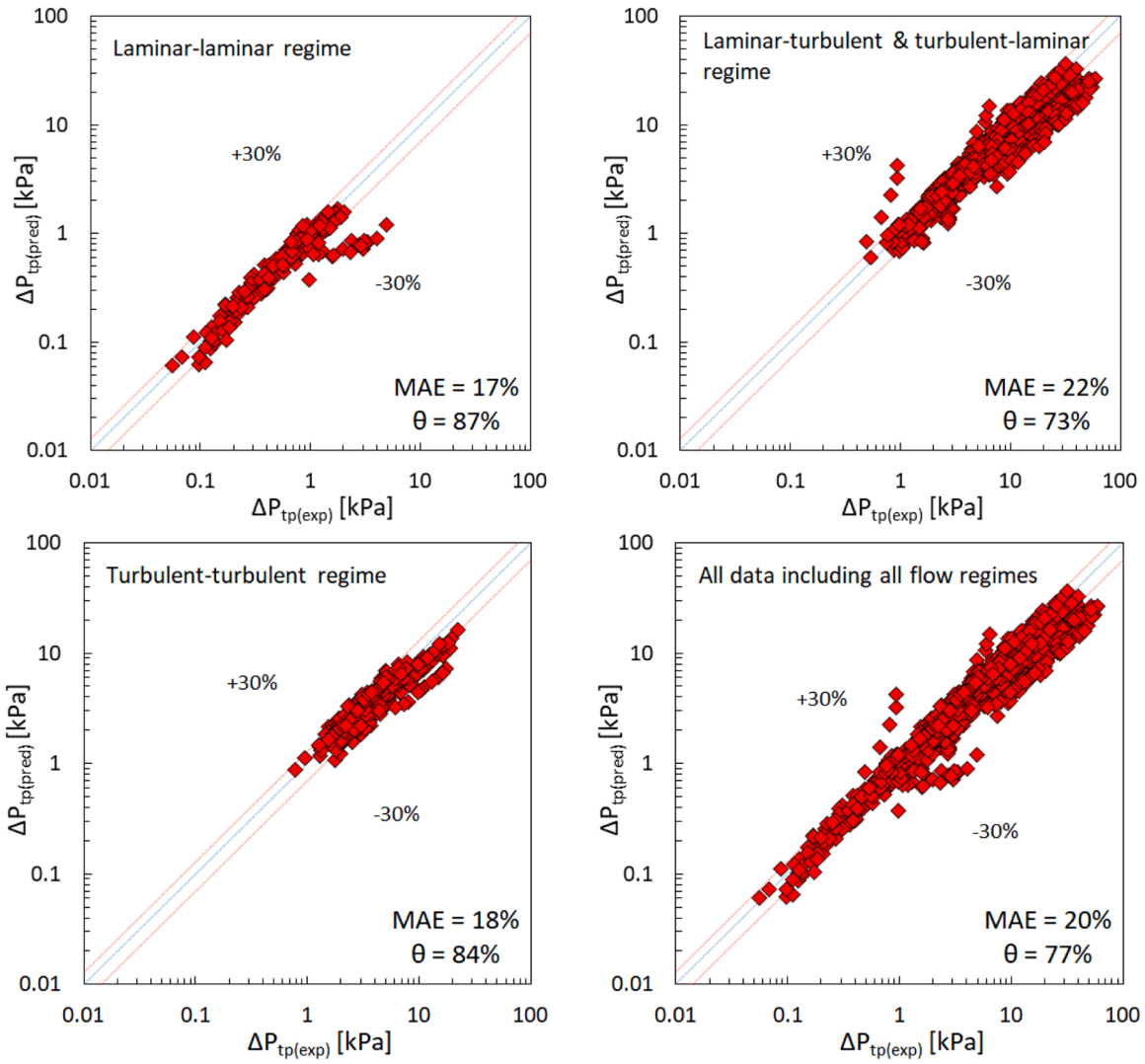

Fig. 12. Comparing graph between the proposed correlation and the experimental data-bank.

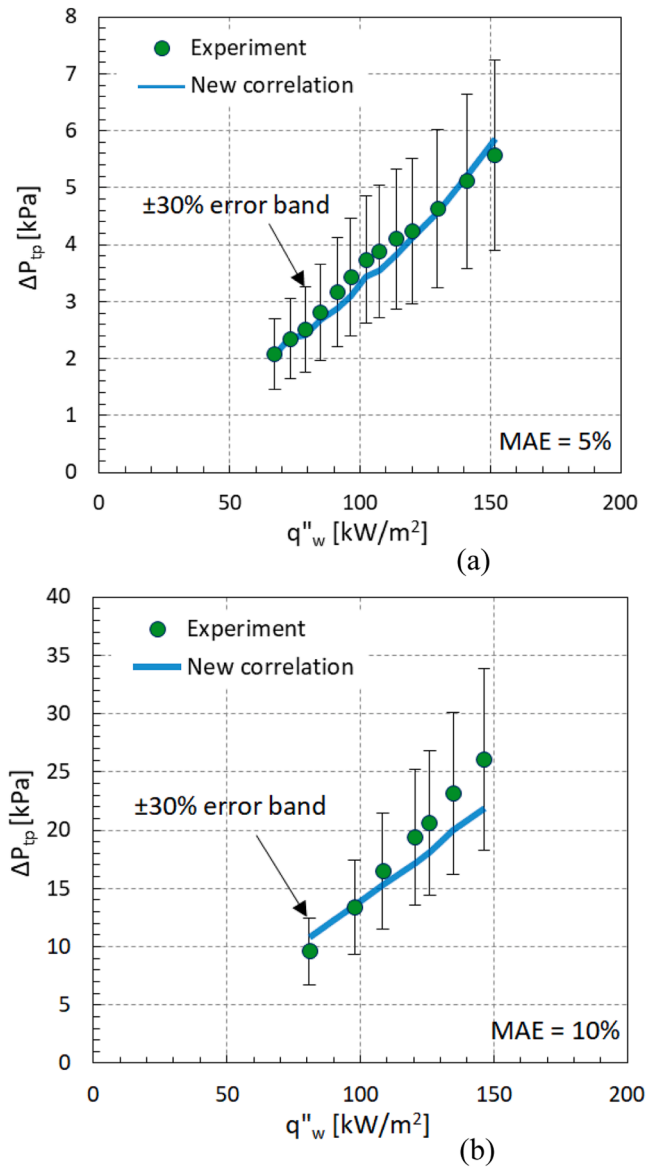

Fig. 13. Trending graph between the proposed correlation and the experimental data points: (a) Multi-channels: HFE-7100, P_i=1 bar, β=0.5, D_h=0.46 mm, G = 250 kg/m^2 s. (b) Single tube: R245fa, P_i=1.8 bar, D_i=2.88 mm, G = 400 kg/m^2 s.

recommended by Qu and Mudawar [28] provided better prediction with the existing data-bank.

4. The sensitivity assessment of different correlations for calculating void fraction showed that, the correlation by Lockhart and Martinelli [30] could be used in the correlations developed for the two-phase pressure drop in small to micro tubes and channels.
5. The prediction of existing correlations was only slightly affected by the choice of different equations for calculating Fanning friction factor. Generally, the equation for a tube (Eq. (5)) and the non-circular correlation by Shah and London [26] can be used in the laminar flow, while the correlations by Blasius [27] proposed for circular channels, can be adopted during the turbulent region in both channel configurations.
6. The Lockhart-Martinelli parameter of four flow regimes should be calculated according to the experimental ranges using the threshold of Reynolds number of 2000. This could provide a better agreement between the experimental results and the existing correlations.
7. By comparing the data points of horizontal rectangular multi-channels, the homogeneous flow model and the correlations by Keepaiboon et al. [46] and Qu and Mudawar [28] provided the smallest MAE, i.e. less than 30 %. However, all the data-bank (including tubes and multi-channels) are not predicted well.
8. The dominant parameters in this data-bank were found to be the Boiling number and the Lockhart–Martinelli parameter. These two parameters showed a clear influence on the experimental flow boiling pressure drop. The present data-bank was then correlated to produce a new correlation for calculating the liquid only two-phase multiplier. This can be used with the frictional component to predict the two-phase pressure drop in small to micro scale single and multi-channels. The new proposed correlation provided a MAE of 20 %, and it is recommended to design heat sinks and small tubes within the range covered.
9. The effect of inlet sub-cooling needs to be examined for further performance enhancement. This could also include a wide range of different working fluids and different surface characteristics due to different coatings or manufacturing process (milling or additive). The new data could be used to assess the new correlation.

7. Author statement

T. G. Karayiannis planned the project. M. M. Mahmoud designed and constructed the test rig. A. H. Al-Zaidi designed and constructed the test section and recommissioned the experimental facility under the supervision of T.G. Karayiannis. A. H. Al-Zaidi carried out the experiments and presented the results and first draft for changes and additions to T.G. Karayiannis and M. M. Mahmoud. All authors discussed the results and contributed to corrections and changes, leading to the final manuscript.

CRediT authorship contribution statement

Ali H. Al-Zaidi: Data curation, Formal analysis, Investigation, Validation, Visualization, Writing – original draft, Writing – review & editing. **Mohamed M. Mahmoud:** Data curation, Formal analysis, Writing – review & editing. **Tassos G. Karayiannis:** Conceptualization, Data curation, Formal analysis, Funding acquisition, Investigation, Methodology, Project administration, Resources, Supervision, Validation, Visualization, Writing – review & editing.

Declaration of competing interest

The authors declare that they have no known competing financial interests or personal relationships that could have appeared to influence the work reported in this paper.

Data availability

Data will be made available on request.

Acknowledgements

The authors would like to thank the support of the Engineering and Physical Sciences Research Council (EPSRC) through grant (EP/K01112/1) and the current grant of (EP/P004709/1).

Appendix I Pressure drop correlations

Single Channel:

Author(s)	Frictional Component	Gravitational and Acceleration Components	Lockhart–Martinelli Parameter	Remarks
Lockhart and Martinelli [30]	Use Eq. (12) and: C = 5 (for laminar liquid-laminar vapour) C = 12 (for laminar liquid-turbulent vapour) C = 10 (for turbulent liquid- laminar vapour) C = 20 (for turbulent liquid-turbulent vapour)	Use Eq. (10–11) and the void fraction by Lockhart and Martinelli from Table 2	X_{lt} or X_{tl} defined in Table 3	Circular channels, horizontal flow D_h: 1.5 – 25.8 mm Air-water, air-benzene, air-kerosene and air-oils
Mishima and Hibiki [32]	Use Eq. (12) and: $C = 21(1 - e^{-0.319*10^3 D_h})$	Use Eq. (10–11) and the void fraction by Lockhart and Martinelli from Table 2	X_{ll} defined in Table 3	Circular and rectangular channels, horizontal/vertical flow D_h: 1.05–4.08 mm Air-water, ammonia, R113-N2
Yu et al. [72]	Use Eq. (12) and: For laminar liquid-turbulent gas: $\varnothing_l^2 = \frac{1}{X^{1.9}}$	Use Eq. (10–11) and the void fraction by Zivi from Table 2	$X = 18.65\left(\frac{Re_{gs}^{0.1}}{Re_{ls}^{0.5}}\right)\left(\frac{1-x}{x}\right)\left(\frac{\rho_g}{\rho_l}\right)^{0.5}$	Circular channels, horizontal flow D_h: 2.98 mm Water
Keepaiboon et al. [46]	Use Eq. (12) and: $C = 1.93 * 10^5 Re_{lo}^{-1.18} Co^{-27.99} X^{0.93}$	Use Eq. (10–11) and the void fraction by Zivi from Table 2	X_{lt} or X_{tl} defined in Table 3	Rectangular channels, horizontal flow D_h: 0.68 mm R134a
Hwang and Kim [65]	Use Eq. (12) and: $C = 0.227 Re_{lo}^{0.452} X^{-0.32} Co^{-0.82}$	Use Eq. (10–11) and the void fraction by Lockhart and Martinelli from Table 2	X_{lt} or X_{tl} defined in Table 3	Circular channels, horizontal flow D_h: 0.24, 0.43 & 0.79 mm R134a
Lee and Lee [69]	Use Eq. (12) and: For laminar liquid and turbulent vapour: $C = 6.185 \times 10^{-2} Re_{lo}^{0.726}$ For turbulent liquid and laminar vapour: $C = 3.627 Re_{lo}^{0.174}$ For turbulent liquid and turbulent vapour: $C = 0.408 Re_{lo}^{0.451}$	Use Eq. (10–11) and the void fraction by Zivi from Table 2	X_{lt} or X_{tl} defined in Table 3	Rectangular channels, horizontal flow D_h: 0.78–6.67 mm Air-water mixture
Pamitran et al. [16]	Use Eq. (12) and: $C = 3 \times 10^{-3} We_{tp}^{-0.433} Re_{tp}^{1.23}$ $We_{tp} = \frac{G^2 D_h}{\sigma \rho_{tp}}$, $Re_{tp} = \frac{G D_h}{\mu_{tp}}$ $\rho_{tp} = \alpha\rho_g + (1-\alpha)\rho_l$ $\mu_{tp} = \mu_l(1-A)(1+2.5A) + \mu_g A$ $A = \frac{x}{(x+(1-x)\rho_g/\rho_l)}$ For $Re_{ks} < 2000$: $f_k = \frac{16}{Re_{ks}}$ For $Re_{ks} > 2000$: $f_k = \frac{0.079}{Re_{ks}^{0.25}}$ (k) refers to liquid (l) or vapour (g)	Use Eq. (10–11) and the void fraction by Rouhani and Axelsson from Table 2	X_{lt} or X_{tl} defined in Table 3	Circular channels, horizontal flow D_h: 0.5–3 mm R134a, R410A, R290, R744, R22

Multi-channels:

Author(s)	Frictional Component	Gravitational and Acceleration Components	Lockhart–Martinelli Parameter	Remarks
Raju et al. [55]	Use Eq. (12) and: $\varnothing_l^2 = 1 + \frac{25}{X} + \frac{3}{X^2}, f_k = \frac{3.119}{Re_{ks}^{0.55}}$ (k) refers to (l) for liquid or (g) for vapour	Use Eq. (10–11) and the homogeneous void fraction from Table 2	X_{lt} or X_{tl} defined in Table 3	Rectangular (wavy channels) channels, vertical flow D_h: 2.3 mm R134a
Qu and Mudawar [28]	Use Eq. (12) and: $C = 21(1 - e^{-319*D_h})(0.00418G + 0.0613)$	Use Eq. (10–11) and the void fraction by Zivi from Table 2	X_{ll} defined in Table 3	Rectangular channels, horizontal flow D_h: 0.35 mm Water
Lee and Garimella [1]	Use Eq. (12) and: $C = 2566 G^{0.5466} D_h^{0.8819} (1 - e^{-319 D_h})$	Use Eq. (10–11) and the void fraction by Zivi from Table 2	X_{ll} defined in Table 3	Rectangular channels, horizontal flow D_h: 0.16–0.57 mm Water

(continued on next page)

(*continued*)

Huang and Thome [42]	Use Eq. (12) and: For $Re_{ls} \leq 2000$ and $Re_{gs} \leq 2000$: $C = 0.0037 Re_{gs}^{1.7} Re_{lo}^{-0.83}$ For $Re_{ls} \leq 2000$ and $Re_{gs} > 2000$: $C = 0.9 Re_{gs}^{0.034} Re_{lo}^{0.2}$ For $Re_{ks} \leq 2000$ and R1233zd(E): $f_k = \frac{8.058}{Re_{ks}}$ For $Re_{ks} \leq 2000$ and others: $f_k * Re_{ks} = 24(1 - 1.355\beta + 1.946\beta^2 - 1.7012\beta^3 + 0.9564\beta^4 - 0.2537\beta^5)$ For $Re_{ks} > 2000$: $f_k = \frac{0.079}{Re_{ks}^{0.25}}$ (k) refers to (l) for liquid or (g) for vapour	Use Eq. (10–11) and the void fraction by Zivi from Table 2	X_{lt} or X_{tl} defined in Table 3	Square channels, horizontal flow D_h: 0.1 mm R1233zd(E), R245fa and R236fa
Markal et al. [56]	Use Eq. (12) and: $C = -7.1 + \left(\frac{(1-x_o)^{1.766}}{Re_{lo}^{0.12} \beta^{0.031} Bo^{0.165} We_{lo}^{0.074} \left(\frac{\nu_l}{\nu_g}\right)^{0.233} \left(\frac{L_{tp}}{D_h}\right)^{0.247}} \right)$	Use Eq. (10–11) and the void fraction by Zivi from Table 2	X_{lt} or X_{tl} defined in Table 3	Rectangular channels, horizontal flow D_h: 0.1–0.25 mm Water
Warrier et al. [45]	Use Eq. (12) and: For all flow regions: C = 38	Use Eq. (10–11) and the void fraction by Lockhart and Martinelli from Table 2	X_{lt} or X_{tl} defined in Table 3	Rectangular channels, horizontal flow D_h: 0.75 mm FC-84
Lee and Mudawar [70]	Use Eq. (12) and: For laminar liquid-laminar gas: $C = 2.16 Re_{lo}^{0.047} We_{lo}^{0.6}$ For laminar liquid- turbulent gas: $C = 1.45 Re_{lo}^{0.25} We_{lo}^{0.23}$	Use Eq. (10–11) and the void fraction by Zivi from Table 2	X_{lt} or X_{tl} defined in Table 3	Rectangular channels, horizontal flow D_h: 0.35 mm R134a
Choi et al. [47]	Use Eq. (12) and: $C = 0.05 Re_{lo}^{0.68} We_{lo}^{-0.34} X^{-1.32}$	Use Eq. (10–11) and the void fraction by Zivi from Table 2	X_{tt} defined in Table 3	Rectangular channels, horizontal flow D_h: 0.27 mm FC-72
Huang et al. [41]	Use Eq. (12) and: $C = 21\left[1 - exp\left(-\frac{0.358}{La}\right)\right](0.06548 j_g + 0.17033)$ $j_g = \frac{Gx}{\rho_g}$, $La = \sqrt{\frac{\sigma}{g\Delta\rho D_h^2}}$	Use Eq. (10–11) and the void fraction by Zivi from Table 2	X_{lt} or X_{tl} defined in Table 3	Rectangular channels, horizontal flow D_h: 0.55 mm R134a
Li and Hibiki [49]	Use Eq. (12) and: For laminar liquid-laminar vapour: $C = 1.87 Re_{tp}^{0.38} x^{0.35} N\mu_{tp}^{0.12}$ For laminar liquid-turbulent vapour: $C = 2.23 Re_{tp}^{0.54} x^{0.25} N\mu_{tp}^{0.51}$ For turbulent liquid-turbulent vapour: $C = 7.63 Re_{tp}^{0.66} x^{0.43} N\mu_{tp}^{1.2}$ For turbulent liquid-laminar vapour: $C = 1.54 Re_{tp}^{0.52} x^{0.42} N\mu_{tp}^{0.14}$ $Re_{tp} = GD_h/\mu_{tp}$, $\frac{1}{\mu_{tp}} = \frac{1-x}{\mu_l} + \frac{x}{\mu_g}$ $N\mu_{tp} = \frac{\mu_{tp}}{(\rho_{tp}\sigma\sqrt{\sigma/g\Delta\rho})^{0.5}}$, $\rho_{tp} = x\rho_g + (1-x)\rho_l$	Use Eq. (10–11) and the void fraction by Lockhart and Martinelli from Table 2	X_{lt} or X_{tl} defined in Table 3	Rectangular/circular channels, horizontal flow D_h: 0.109–2.13 mm R134a, R22, R404a, R236fa, R245fa, FC-72, CO2, water
Lee et al. [48]	Use Eq. (12) and: $C = 121.6(1 - \exp(-22.7Bd))x^{1.85}$	Use Eq. (10–11) and the void fraction by Zivi from Table 2	X_{lt} or X_{tl} defined in Table 3	Rectangular channels, horizontal flow D_h: 0.35–2.46 mm Water, n-pentane, ammonia, CO2, R410a, R12 and R134a

Single and Multi-channels:

Author(s)	Frictional Component	Gravitational and Acceleration Components	Lockhart–Martinelli Parameter	Remarks
Zhang and Webb [43]	Use Eq. (13) and: $\varnothing_{lo}^2 = (1-x)^2 + 2.87x^2\left(\frac{P_i}{P_{cr}}\right)^{-1} + 1.68x^{0.8}(1-x)^{0.25}\left(\frac{P_i}{P_{cr}}\right)^{-1.64}$	Use Eq. (10–11) and the void fraction by Zivi from Table 2	——	Circular channels, horizontal flow D_h: 2.13, 3.25 & 6.25 mm R134a, R22 and R404a
Kim and Mudawar [59]	Use Eq. (12) and: For $Re_{ls} < 2000$: $C = C^*\left(1 + 530 We_{lo}^{0.52}\left(Bo\frac{P_{er,h}}{P_{er,w}}\right)^{1.09}\right)$ For $Re_{ls} \geq 2000$: $C = C^*\left(1 + 60 We_{lo}^{0.32}\left(Bo\frac{P_{er,h}}{P_{er,w}}\right)^{0.78}\right)$	Use Eq. (10–11) and the void fraction by Zivi from Table 2	X_{lt} or X_{tl} defined in Table 3	Rectangular/circular channels, horizontal/vertical flow D_h: 0.349–5.35 mm R12, R22, R134a, R245fa, R410a, FC-72, CO2, ammonia and water

(*continued on next page*)

(*continued*)

	For $Re_{ls} < 2000$ and $Re_{gs} < 2000$: $C^* = 3.5 * 10^{-5} Re_{lo}^{0.44} Su_{go}^{0.5} \left(\frac{\rho_l}{\rho_g}\right)^{0.48}$ For $Re_{ls} < 2000$ and $Re_{gs} \geq 2000$: $C^* = 0.0015 Re_{lo}^{0.59} Su_{go}^{0.19} \left(\frac{\rho_l}{\rho_g}\right)^{0.36}$ For $Re_{ls} \geq 2000$ and $Re_{gs} < 2000$: $C^* = 8.7 * 10^{-4} Re_{lo}^{0.17} Su_{go}^{0.5} \left(\frac{\rho_l}{\rho_g}\right)^{0.14}$ For $Re_{ls} \geq 2000$ and $Re_{gs} \geq 2000$: $C^* = 0.39 Re_{lo}^{0.03} Su_{go}^{0.1} \left(\frac{\rho_l}{\rho_g}\right)^{0.35}$ Heated perimeter of channel: $P_{er,h} = 2H_{ch} + W_{ch}$ Wetted perimeter of channel: $P_{er,w} = 2H_{ch} + 2W_{ch}$ [The ratio of the flow channel's heated to wetted perimeters ($\frac{P_{er,h}}{P_{er,w}}$) for circular channels: 1]			
Zhang et al. [66]	Use Eq. (12) and: $C = 21\left(1 - exp\left(-\frac{0.358}{La}\right)\right)$, $La = \sqrt{\frac{\sigma}{g\Delta\rho D_h^2}}$	Use Eq. (10–11) and the void fraction by Lockhart and Martinelli from Table 2	X_{lt} or X_{tl} defined in Table 3	Rectangular/circular channels, horizontal/vertical flow D_h: 0.007–6.25 mm Air-water, R113-N2, water-N2, air-ethanol, air-oil, ammonia, R134a, R22, R404a, R236ea, R410A, R12
Li and Wu [67]	Use Eq. (12) and: For $Bd \leq 1.5$, $C = 11.9 Bd^{0.45}$ For $1.5 < Bd \leq 11$ $C = 109.4 (Bd * Re_{ls}^{0.5})^{-0.56}$	Use Eq. (10–11) and the void fraction by Lockhart and Martinelli from Table 2	X_{lt} or X_{tl} defined in Table 3	Rectangular/circular channels, horizontal/vertical flow D_h: 0.148–3.25 mm Ammonia, propane, R404a, R22, R12, R410a, R236ea, R245fa, R422d, N2, R32 and R134a
Sun and Mishima [68]	Use Eq. (12) and: For $Re_{ls} \leq 2000$ and $Re_{gs} \leq 2000$: $C = 26\left(1 + \frac{Re_{ls}}{1000}\right)\left(1 - \exp\left(\frac{-0.153}{0.8 + 0.27La}\right)\right)$ $La = \sqrt{\frac{\sigma}{g\Delta\rho D_h^2}}$ For $Re_{ls} > 2000$ and $Re_{gs} > 2000$: $C = 1.79\left(\frac{Re_{gs}}{Re_{ls}}\right)^{0.4} \left(\frac{1-x}{x}\right)^{0.5}$	Use Eq. (10–11) and the void fraction by Zivi from Table 2	X_{lt} or X_{tl} defined in Table 3	Rectangular/circular channels, horizontal/vertical flow D_h: 0.506–12 mm Air-water, CO2, R123, R22, R236ea, R245fa, R404A, R407C, R410A, R507 and R134a
Zeng et al. [44]	Use Eq. (13) and: $\varnothing_{lo}^2 = [1 + (-45,716) Fr^{0.5305} Bo^{0.848} Re_{tp}^{-1.2326} (X^2 - 1) x](1 - x^{2.794})^{0.672} + X^2 x^{0.8517}$ $Re_{tp} = E * Re_{ls} + Re_{gs}$ $E = -0.89 + 0.95 X_{tt}^{-0.923} \left(\frac{\rho_g}{\rho_l}\right)^{-0.0198} - 14.8 We_{lo}^{0.22} Bo^{0.303} Fr^{-0.62}$ $X_{tt} = \left(\frac{\mu_l}{\mu_g}\right)^{0.1} \left(\frac{1-x}{x}\right)^{0.9} \left(\frac{\rho_g}{\rho_l}\right)^{0.5}$ For $Re_{lo} \leq 1187$: $f_{lo} = \frac{16}{Re_{lo}}$ For $Re_{lo} > 1187$: $f_{lo} = \frac{0.079}{Re_{lo}^{0.25}}$	Use Eq. (10–11) and the void fraction by Zivi from Table 2	X_{lt} or X_{tl} defined in Table 3	Circular channels, horizontal flow D_h: 0.643–6 mm R32
Moradkhani et al. [71]	Use Eq. (13) and: For Bd < 3: $\varnothing_{lo}^2 = \left(\frac{P_i}{P_{cr}}\right) + \frac{1.352\,x}{H} + \min(A_1, A_2)$ For $Bd \geq 3$: $\varnothing_{lo}^2 = x + 7\left(\frac{P_i}{P_{cr}}\right) + 1.456 \frac{sin(sin(x))}{H} + \frac{x}{2.67 \times 10^{-3} Bd + 227.68\left[0.651^{sin\left(7.42\frac{(P_i/P_{cr})}{H}\right)}\right]}$ $A_1 = \frac{8x}{Bd^2 H} + exp\left(2\tan\left(\frac{P_i}{P_{cr}}\right)\right)$ $A_2 = 1.0937^{R.Bd}$, $H = \left(\frac{f_{lo}}{f_{go}}\right)\left(\frac{\rho_g}{\rho_l}\right)$	Use Eq. (10–11) and the void fraction by Zivi from Table 2	——	Rectangular/circular channels, horizontal/vertical flow D_h: 0.07–14 mm R717, R245fa, R290, R600a, R744, R1234yf, R134a, R718, R32, R410A, R1234ze(E), R1270, R404A, R22, R12, Ethanol

(*continued on next page*)

(*continued*)

$$R = \left(\frac{Re_{go}}{Re_{lo}}\right),$$

For $Re_{ko} < 2000$: $f_{ko} = \dfrac{16}{Re_{ko}}$

For $2000 \le Re_{ko} < 20{,}000$: $f_{ko} = \dfrac{0.079}{Re_{ko}^{0.25}}$

For $Re_{ko} \ge 20{,}000$: $f_{ko} = \dfrac{0.046}{Re_{ko}^{0.2}}$

(k) refers to (l) for liquid or (g) for vapour

References

[1] P. Lee, S.V. Garimella, Saturated flow boiling heat transfer and pressure drop in silicon microchannel arrays, Int. J. Heat Mass Transf. 51 (3) (2008) 789–806.
[2] M.M. Mahmoud, T.G. Karayiannis, D.B.R. Kenning, Flow boiling pressure drop of R134a in microdiameter tubes: Experimental results and assessment of correlations, Heat Transf. Eng. 35 (2) (2014) 178–192.
[3] B. Markal, O. Aydin, M. Avci, An experimental investigation of saturated flow boiling heat transfer and pressure drop in square microchannels, Int. J. Refrig. 65 (2016) 1–11.
[4] V.Y.S. Lee, A. Al-Zaidi, G. Henderson, T.G. Karayiannis, Flow boiling results of hfe-7200 in a multi-microchannel evaporator and comparison with HFE-7100, in: Proceedings of the 4th World Congress on Momentum, Heat and Mass Transfer (MHMT 19), 2019, pp. 1–10.
[5] T. Harirchian, S.V. Garimella, Microchannel size effects on local flow boiling heat transfer to a dielectric fluid, Int. J. Heat Mass Transf. 51 (15–16) (2008) 3724–3735.
[6] Y. Xu, X. Fang, D. Li, G. Li, Y. Yuan, A. Xu, An experimental study of flow boiling frictional pressure drop of R134a and evaluation of existing correlations, Int. J. Heat Mass Transf. 98 (2016) 150–163.
[7] L. Yin, P. Jiang, R. Xu, H. Hu, L. Jia, Heat transfer and pressure drop characteristics of water flow boiling in open microchannels, Int. J. Heat Mass Transf. 137 (2019) 204–215.
[8] C.J. Kuo, Y. Peles, Pressure effects on flow boiling instabilities in parallel microchannels, Int. J. Heat Mass Transf. 52 (1–2) (2009) 271–280.
[9] S. Saisorn, J. Kaew-On, S. Wongwises, Flow pattern and heat transfer characteristics of R-134a refrigerant during flow boiling in a horizontal circular mini-channel, Int. J. Heat Mass Transf. 53 (19–20) (2010) 4023–4038.
[10] E.R. Dário, J.C. Passos, M.L. Sánchez Simón, L. Tadrist, Pressure drop during flow boiling inside parallel microchannels, Int. J. Refrig. 72 (2016) 111–123.
[11] V.Y.S. Lee, T.G. Karayiannis, Influence of system pressure on flow boiling in microchannels, Int. J. Heat Mass Transf. 215 (2023) 124470.
[12] D. Deng, W. Wan, H. Shao, Y. Tang, J. Feng, J. Zeng, Effects of operation parameters on flow boiling characteristics of heat sink cooling systems with reentrant porous microchannels, Energy Convers. Manag. 96 (2015) 340–351.
[13] J. Chen, S. Zhang, Y. Tang, H. Chen, W. Yuan, J. Zeng, Effect of operational parameters on flow boiling heat transfer performance for porous interconnected microchannel nets, Appl. Therm. Eng. 121 (2017) 443–453.
[14] V.Y.S. Lee, T.G. Karayiannis, Effect of Inlet Subcooling on Flow Boiling in Microchannels, Appl. Therm. Eng. 181 (2020) 115966.
[15] R. Revellin, J.R. Thome, Adiabatic two-phase frictional pressure drops in microchannels, Exp. Therm. Fluid Sci. 31 (7) (2007) 673–685.
[16] A.S. Pamitran, K. Il Choi, J.T. Oh, P. Hrnjak, Characteristics of two-phase flow pattern transitions and pressure drop of five refrigerants in horizontal circular small tubes, Int. J. Refrig. 33 (3) (2010) 578–588.
[17] S.G. Singh, A. Kulkarni, S.P. Duttagupta, B.P. Puranik, A. Agrawal, Impact of aspect ratio on flow boiling of water in rectangular microchannels, Exp. Therm. Fluid Sci. 33 (1) (2008) 153–160.
[18] B.T. Holcomb, T. Harirchian, S.V. Garimella, An experimental investigation of microchannel size effects on flow boiling with de-ionized water, in: Proceedings of the ASME 2009 Heat Transfer Summer Conference, San Francisco, California USA, 2009, pp. 1–9.
[19] K.P. Drummond, D. Back, M.D. Sinanis, D.B. Janes, D. Peroulis, J.A. Weibel, S. V. Garimella, A hierarchical manifold microchannel heat sink array for high-heat-flux two-phase cooling of electronics, Int. J. Heat Mass Transf. 117 (2018) 319–330.
[20] A.H. Al-Zaidi, M.M. Mahmoud, T.G. Karayiannis, Effect of aspect ratio on flow boiling characteristics in microchannels, Int. J. Heat Mass Transf. 164 (2021) 120587.
[21] B.J. Jones, S.V. Garimella, Surface roughness effects on flow boiling in microchannels, J. Therm. Sci. Eng. Appl. 1 (4) (2009).
[22] R. Jafari, T. Okutucu-Özyurt, H.Ö. Ünver, Ö. Bayer, Experimental investigation of surface roughness effects on the flow boiling of R134a in microchannels, Exp. Therm. Fluid Sci. 79 (2016) 222–230.
[23] E.A. Pike-Wilson, T.G. Karayiannis, Flow boiling of R245fa in 1.1 mm diameter stainless steel, brass and copper tubes, Exp. Therm. Fluid Sci. 59 (2014) 166–183.
[24] A.H. Al-Zaidi, M.M. Mahmoud, T.G. Karayiannis, Flow boiling in copper and aluminium microchannels, Int. J. Heat Mass Transf. 194 (2022) 123101.
[25] J.G. Collier, J.R. Thome, Convective Boiling and Condensation, Third edit, Oxford University Press, Oxford, UK, 1994.
[26] R.K. Shah, A.L. London, Laminar Flow Forced Convection in ducts, Supplement 1 to Advances in Heat Transfer, Academic Press, New York, 1978.
[27] H. Blasius, Das Ähnlichkeitsgesetz bei Reibungsvorgängen in Flüssigkeiten. Mitteilungen über Forschungsarbeiten Auf Dem Gebiete des Ingenieurwesens, Springer Berlin Heidelb, 1913, p. 131.
[28] W. Qu, I. Mudawar, Measurement and prediction of pressure drop in two-phase micro-channel heat sinks, Int. J. Heat Mass Transf. 46 (15) (2003) 2737–2753.
[29] S.M. Zivi, Estimation of steady-state steamvoid-fraction by means of the principle of minimum entropy production, J. Heat Transf. 86 (1964) 247–252.
[30] R.W. Lockhart, R.C. Martinelli, Proposed correlation of data for isothermal two-phase, two-component flow in pipes, Chemical Engineering Progress 45 (1) (1949) 39–48.
[31] D. Chisholm, A theoretical basis for the Lockhart–Martinelli correlation for two-phase flow, Int. J. Heat Mass Transf. 10 (1967) 1767–1778.
[32] K. Mishima, T. Hibiki, Some characteristics of air-water two-phase flow in small diameter vertical tubes, Int. J. Multiph. Flow 22 (4) (1996) 703–712.
[33] X. Huo, L. Chen, Y.S. Tian, T.G. Karayiannis, Flow boiling and flow regimes in small diameter tubes, Appl. Therm. Eng. 24 (8–9) (2004) 1225–1239.
[34] D. Shiferaw, T.G. Karayiannis, D.B.R. Kenning, Flow boiling in a 1.1 mm tube with R134a: Experimental results and comparison with model, Int. J. Therm. Sci. 48 (2) (2009) 331–341.
[35] A.M. Al-Gaheeshi, PhD thesis, Brunel University London, 2018.
[36] R.K. Shah, D.P. Sekulić, Fundamentals of Heat Exchanger Design, John Wiley Sons Inc, 2003.
[37] S.G. Kandlikar, W.J. Grande, Evolution of microchannel flow passages—Thermo hydraulic performance and fabrication technology, Heat Transf. Eng. 25 (1) (2003) 3–17.
[38] T.G. Karayiannis, M.M. Mahmoud, Flow boiling in microchannels: Fundamentals and applications, Appl. Therm. Eng. 115 (2017) 1372–1397.
[39] T. Harirchian, S.V. Garimella, A comprehensive flow regime map for microchannel flow boiling with quantitative transition criteria, Int. J. Heat Mass Transf. 53 (13) (2010) 2694–2702.
[40] N. Brauner, D.M. Maron, Identification of the range of 'small diameters' conduits, regarding two-phase flow pattern transitions, Int. Commun. Heat Mass Transf. 19 (1) (1992) 29–39.
[41] Y. Huang, B. Shu, S. Zhou, Q. Shi, Experimental investigation and prediction on pressure drop during flow boiling in horizontal microchannels, Micromachines 12 (510) (2021) 1–17.
[42] H. Huang, J.R. Thome, An experimental study on flow boiling pressure drop in multi-microchannel evaporators with different refrigerants, Exp. Therm. Fluid Sci. 80 (2017) 391–407.
[43] M. Zhang, R.L. Webb, Correlation of two-phase friction for refrigerants in small-diameter tubes, Exp. Therm. Fluid Sci. 25 (2001) 131–139.
[44] W. Zeng, B. Gu, Z. Du, X. Liu, Z. Tian, New generalized flow boiling heat transfer and frictional pressure drop correlations for R32, Int. J. Refrig. 131 (2021) 634–644.
[45] G.R. Warrier, V.K. Dhir, L.A. Momoda, Heat transfer and pressure drop in narrow rectangular channels, Exp. Therm. Fluid Sci. 26 (2002) 53–64.
[46] C. Keepaiboon, P. Thiangtham, O. Mahian, A.S. Dalkiliç, S. Wongwises, Pressure drop characteristics of R134a during flow boiling in a single rectangular micro-channel, Int. Commun. Heat Mass Transf. 71 (2016) 245–253.
[47] Y. Choi, T. Lim, S. You, H. Kim, Pressure drop characteristics for two-phase flow of FC-72 in microchannel, J. Mech. Eng. Sci. 232 (6) (2017) 987–997.
[48] H.J. Lee, D.Y. Liu, Y. Alyousef, S. chune Yao, Generalized two-phase pressure drop and heat transfer correlations in evaporative micro /minichannels, J. Heat Transfer 132 (2010) 1–9.
[49] X. Li, T. Hibiki, Frictional pressure drop correlation for two-phase flows in mini and micro multi-channels, Appl. Therm. Eng. 116 (2017) 316–328.
[50] W.H. McAdams, W. W.K, H. L.C, Vaporization inside horizontal tubes-II Benzene-oil mixtures, ASME Trans. 64 (1942) 193–200.
[51] A. Cicchitti, C. Lombardi, M. Silvestri, G. Soldaini, R. Zavattarelli, Two-phase cooling experiments: pressure drop, heat transfer and burnout measurements, Energ. Nucl. 7 (6) (1959) 407–425.
[52] W.L. Owens, Two-phase pressure gradient. Int. Dev. Heat Transf. Pt. II, ASME, New York, 1961.
[53] S.Z. Rouhani, E. Axelsson, Calculation of void volume fraction in the subcooled and quality boiling regions, Int. J. Heat Mass Transf. 13 (2) (1970) 383–393.
[54] D. Chisholm, Pressure gradients due to friction during the flow of evaporating two-phase mixtures in smooth tubes and channel, Int. J. Heat Mass Transf. 16 (29) (1973) 347–358.

[55] M.A. Raju, T.P.A. Babu, C. Ranganayakulu, Investigation of fl ow boiling heat transfer and pressure drop of R134a in a rectangular channel with wavy fin, Int. J. Therm. Sci. 147 (2020) 106055.
[56] B. Markal, O. Aydin, M. Avci, Prediction of pressure drop for flow boiling in rectangular multi-microchannel heat sinks, Heat Transf. Eng. (2017) 1–13, vol. 0, no. 0.
[57] B.S. Petukhov, Heat transfer and friction in turbulent pipe flow with variable physical properties, in: Adv. Heat Transf., 6, Acad. Press, New York, 1970, pp. 503–565.
[58] R.J. Phillips, Forced-Convection,Liquid-Cocled,Micrichannel Heat Sinks, Massachusetts Institute of Technology (1987).
[59] S.M. Kim, I. Mudawar, Universal approach to predicting two-phase frictional pressure drop for mini/micro-channel saturated flow boiling, Int. J. Heat Mass Transf. 58 (1–2) (2013) 718–734.
[60] P.A. Kew, K. Cornwell, Correlations for the prediction of boiling heat transfer in small diameter channels, Appl. Therm. Eng. 17 (1997) 705–715.
[61] K.A. Triplett, S.M. Ghiaasiaan, S.I. Abdel-Khalik, D.L. Sadowski, Gas–liquid two-phase flow in microchannels Part I: two-phase flow patterns, Int. J. Multiph. Flow 25 (3) (1999) 377–394.
[62] A. Ullmann, N. Brauner, The prediction of flow pattern maps in minichannels, Multiph. Sci. Technol. 19 (1) (2007) 49–73.
[63] C.L. Ong, J.R. Thome, Macro-to-microchannel transition in two-phase flow: Part 1 - Two-phase flow patterns and film thickness measurements, Exp. Therm. Fluid Sci. 35 (1) (2011) 37–47.
[64] C.B. Tibiriçá, G. Ribatski, Flow boiling phenomenological differences between micro- and macroscale channels, Heat Transf. Eng. 36 (11) (2015) 937–942.
[65] Y.W. Hwang, M.S. Kim, The pressure drop in microtubes and the correlation development, Int. J. Heat Mass Transf. 49 (2006) 1804–1812.
[66] W. Zhang, T. Hibiki, K. Mishima, Correlations of two-phase frictional pressure drop and void fraction in mini-channel, Int. J. Heat Mass Transf. 53 (2010) 453–465.
[67] W. Li, Z. Wu, A general correlation for adiabatic two-phase pressure drop in micro/mini-channels, Int. J. Heat Mass Transf. 53 (13) (2010) 2732–2739.
[68] L. Sun, K. Mishima, Evaluation analysis of prediction methods for two-phase flow pressure drop in mini-channels, Int. J. Multiph. Flow 35 (1) (2009) 47–54.
[69] H.J. Lee, S.Y. Lee, Pressure drop correlations for two-phase flow within horizontal rectangular channels with small heights, Int. J. Multiph. Flow 27 (2001) 783–796.
[70] J. Lee, I. Mudawar, Two-phase flow in high-heat-flux micro-channel heat sink for refrigeration cooling applications: Part II - Heat transfer characteristics, Int. J. Heat Mass Transf. 48 (5) (2005) 941–955.
[71] M.A. Moradkhani, S.H. Hosseini, P. Morshedi, M. Rahimi, S. Mengjie, Saturated flow boiling inside conventional and mini/micro channels: A new general model for frictional pressure drop using genetic programming, Int. J. Refrig. 132 (2021) 197–212.
[72] W. Yu, D.M. France, M.W. Wambsganss, J.R. Hull, Two-phase pressure drop, boiling heat transfer, and critical heat flux to water in a small-diameter horizontal tube, Int. J. Multiph. Flow 28 (2002) 927–941.